REVIEW ARTICLE

Neoplasia • Vol. 2, Nos. 1–2, January-April 2000, pp. 71–88 71

www.nature.com/neo

Characterizing Tumors Using Metabolic Imaging: PET Imaging of Cellular Proliferation and Steroid Receptors[1]

David A. Mankoff, Farrokh Dehdashti† and Anthony F. Shields‡*

*Division of Nuclear Medicine, Department of Radiology, University of Washington, Seattle, WA; †Mallinckrodt Institute of Radiology, Washington University, Saint Louis, MO and ‡Barbara-Ann Karmanos Cancer Institute, Wayne State University, Detroit, MI

Abstract

Treatment decisions in oncology are increasingly guided by information on the biologic characteristics of tumors. Currently, patient-specific information on tumor biology is obtained from the analysis of biopsy material. Positron emission tomography (PET) provides quantitative estimates of regional biochemistry and receptor status and can overcome the sampling error and difficulty in performing serial studies inherent with biopsy. Imaging using the glucose metabolism tracer, 2-deoxy-2-fluoro-D-glucose (FDG), has demonstrated PET's ability to guide therapy in clinical oncology. In this review, we highlight PET approaches to imaging two other aspects of tumor biology: cellular proliferation and tumor steroid receptors. We review the biochemical and biologic processes underlying the imaging, positron-emitting radiopharmaceuticals that have been developed, quantitative image-analysis considerations, and clinical studies to date. This provides a basis for evaluating future developments in these promising applications of PET metabolic imaging. *Neoplasia* (2000) **2**, 71–88.

Keywords: PET, oncology, response, cellular proliferation, estrogen receptors.

Introduction

One of the recent trends in cancer therapy is to use the biologic characteristics of tumors in formulating individualized treatment plans. Besides the size, location, and extent of the tumor, more specific tumor biologic properties, including measures of cellular proliferation and the expression of particular tumor proteins, can also guide therapy [1]. Examples of biologically based treatment decisions include using the expression of estrogen and progesterone receptors (ERs and PRs) [2,3] and the expression of the HER2/Neu oncogene [4] to select therapy for patients with breast cancer.

The standard cancer work-up includes anatomically based imaging methods, such as computed tomography (CT), magnetic resonance imaging (MR), and ultrasound (US), to determine the extent of tumor by depicting properties such as tumor size, shape, density, vascularity, and relative fat and water content. Specific biologic features such as cellular proliferation and the expression of tumor gene products are determined from the analysis of biopsy material. Although this combination of approaches has yielded some notable successes in treatment planning [3–6], it has important limitations. Anatomically based imaging provides regional information but provides limited functional information and can only differentiate tumors from normal tissue based on shape, density, vascularity, and fat and water content. Analysis of biopsy material provides detailed information on tumor biology but has an inherently limited capacity to determine extent and regional variation. Furthermore, it has significant sampling error due to the macroscopic heterogeneity of large tumors or site-to-site variation in patients with metastases [7–9]. The ability to image regional tumor biology would benefit biologically directed treatment planning and would form a bridge between tissue-based methods of tumor characterization arising from laboratory science and the clinical environment.

To monitor the effectiveness of a chosen treatment, there is an important and complementary need for a timely assessment of response. Treatment-response monitoring is currently based on following changes in tumor size from physical examination or anatomically based imaging [10]. Again, this approach has significant limitations. Reduction in the bulk tumor size is a relatively late consequence of successful therapy. Change in tumor size is preceded by important physiologic and biochemical steps, which include a decrease in tumor cellular proliferation and/or an increase in cellular death rate and a subsequent decline in viable tumor cell number. Decreases in tumor size become notable only after these steps have occurred [1], and it therefore usually takes weeks to months to gauge successful therapy. Furthermore, successful therapy may kill the tumor but leave behind a fibrotic mass. A prime example occurs in treating bulky mediastinal Hodgkins lymphomas [11]. Studies have shown that serial biopsy can detect response earlier than tumor-size measurements and are more accurate in asses-

Address all correspondence to: Dr. David A. Mankoff, MD, PhD, Division of Nuclear Medicine, Box 356113, Room NN203, UWMC, 1959 NE Pacific Street, Seattle, WA 98195.

[1]This work was supported by NIH grants CA42045, CA72064, CA25386, CA39566, and CA82645 and DOE grant DE FG02-84ER60218.

Received 24 September 1999; Accepted 3 November 1999.

sing the degree of response [12–14]. Biopsy, however, is invasive and must be performed at multiple time points to measure response. Again, as in assessing tumor biology, an imaging method that characterizes regional biochemistry should be able to detect response at a much earlier time than anatomically based methods and overcome the inherent limitations of serial biopsy.

Nuclear medicine, the specialty of radionuclide-based tracer imaging methods, is ideally suited to measuring regional biology. Radioisotope imaging can trace biochemical pathways without perturbing native biochemistry using submicromolar quantities of tracers [15]. Competing modalities such as CT or magnetic resonance imaging (MRI) require tracer concentrations that are typically orders of magnitude higher for practical imaging [15]. Radioisotope imaging occurs with little chance of pharmacologic toxicity and minimal radiation burden for the patient. Of available radioisotope imaging methods, positron emission tomography (PET) is a more recently developed radiotracer imaging technique which has significant advantages over conventional single-photon emitting isotope imaging [16,17]. It offers a greater range of radiopharmaceuticals for cancer imaging, provides a superior combination of sensitivity and spatial resolution over single-photon imaging, and allows accurate quantification of dynamic regional tracer concentration [17]. PET has become an increasingly important tool for clinical oncology [16,18–20]. Most clinical PET studies reported to date have used the tracer, 2-deoxy-2-fluoro-D-glucose (FDG). FDG was developed based on earlier work using deoxyglucose to explore brain physiology [21,22]. FDG traces glucose metabolism, a nonspecific process essential for tumor growth but also necessary for inflammatory responses and tissue repair [23,24]. Although the success of FDG PET in oncology has been widely documented, the utility of PET in the management of cancer is not limited to FDG [25]. Other PET tracers have been developed and are targeted to areas of tumor biology which include cellular proliferation [26,27], protein and membrane biosynthesis [28–30], tissue hypoxia [31], and tumor receptor and/or gene product expression [15]. In this review, we highlight two types of PET tracers highly relevant to biologically directed cancer therapy: 1) tracers specifically designed to measure cellular proliferation and 2) tracers designed to measure sex steroid receptors in breast and prostate cancer. These tracers relate to tumor features, namely proliferative rate and hormone receptor expression, for which there is a large body of *in vitro* laboratory and clinical work. Consequently, these are tracers for which it is possible to interpret the results of *in vivo* imaging studies in light of known tumor biology and established clinical treatment paradigms. These tracers would therefore also have rapid translation into clinical practice after validation. We will review the biologic and biochemical principles underlying the imaging studies, review the radiopharmaceuticals that have been developed, discuss issues in the quantitative interpretation of imaging data, and review clinical progress. Because both types of tracers have undergone only preliminary clinical evaluation, we highlight basic science and preclinical work as a basis for understanding the results obtained to date and for predicting future developments.

In reviewing PET imaging of cellular proliferation and tumor receptors, it is important to consider two roles for PET in oncology [17,25,32]: 1) PET provides a powerful clinical tool for cancer treatment planning and therapy monitoring. 2) PET is a unique methodology for examining the "clinical biology" of cancer and can therefore function as a translational bridge between *in vitro* biologic discovery and clinical medicine. Some of the tracers and imaging methods developed in a research setting may be impractical for routine clinical imaging, owing to factors such as short tracer half-life, difficult tracer synthesis, and/or complex imaging protocols. However, failure to investigate radiopharmaceuticals or imaging approaches simply because they are not practical for everyday use in the clinic would deprive medical science of potentially valuable tools for understanding how cancer behaves *in vivo*. Techniques such as PET will be important in helping to select from a vast array of new therapeutic approaches, both by investigating response mechanisms in preclinical studies and by providing endpoints for clinical trials [32,33].

Pet Imaging of Cellular Proliferation

Proliferation: Biology and Biochemistry

Cellular proliferation and tumors Uncontrolled proliferation is one of the characteristic features of malignant tumors. Information on growth rates can by inferred by determining the fraction of cells going through mitosis; however, conventional anatomic pathology is limited in its ability to quantify the rate of cellular proliferation. Nevertheless, it became clear that measurement of proliferation provided a means for characterizing tumor behavior and for directly measuring changes in tumor growth in response to therapy [13,34]. Over the years, a variety of techniques have been developed to measure tumor growth rates aimed at characterizing tumor behavior and response to therapy; however, most relied on the use of tissue specimens, limiting the material available for study and making it difficult to obtain serial measurements to follow response. New imaging modalities now offer the opportunity to measure tumor growth noninvasively and repeatedly. This provides a tool for early assessment of response to therapy as well as a means of characterizing response to therapies which may be cytostatic, as opposed to cyotoxic. In the case of cytostatic agents, treatment will not alter the quantity of viable tumor; therefore measuring changes cellular proliferation may be the only effective means of assessing therapeutic success [27,33].

Labeled thymidine to measure cellular proliferation The DNA synthetic pathway requires four nucleoside triphosphates (TTP, ATP, CTP, and GTP) to synthesize DNA. Because thymidine is the only base that is not also incorporated into

RNA, it is the logical choice for cell growth measurements [35]. Growth measurements are accomplished by the introduction of labeled thymidine into the medium of cells grown in culture or by intravenous injection in animals. Labeled thymidine nucleotides (TMP, TDP, TTP) are not useful as tracers because they do not cross the cell membrane. Thymidine, however, is rapidly transported by cells using a facilitated, non–energy-dependent transporter that produces equilibration within seconds [36]. Once it is intracellular, thymidine can be phosphorylated by thymidine kinase (TK) to TMP, and sequentially converted to TTP before use in DNA synthesis. This is called the exogenous (salvage) pathway because it allows the cell to use sources of thymidine produced elsewhere [34,35]. Most of the thymidine used by cells is produced by endogenous (*de novo*) synthesis from uracil. This pathway converts deoxyuridine monophosphate to TMP using thymidylate synthase (TS). It is notable that both TK and TS are closely regulated by cells; the levels of both generally go up 5- to 10-fold as the cells enter S phase [34,35].

Many of the first studies to measure growth were done with tritiated thymidine [35,37] injected into animals before tumor removal. After tumors were excised and fixed, histologic sections were placed on slides and autoradiographed with films of photographic emulsion to record emissions from the tritium. Microscopic examination of the exposed sections yielded estimates of the fraction of cells incorporating thymidine into their DNA at time of injection, i.e., the fraction in S phase [35,37]. This analysis measured the fraction of cells actively replicating, but did not tell one how fast cells were moving through the cell cycle. Counting silver grains over the cells could have provided quantitative estimates of DNA synthesis, but it was very tedious. Scintillation counting and quantitative autoradiography provided more efficient methods of measuring the total radioactivity incorporated into a volume of tumor as a measure of cell growth. However, they shared the same limitations for clinical studies, namely the need for tumor biopsies and the radiation burden of a long-lived tracer. Radiotracer techniques, in particular PET, offer a noninvasive approach to quantifying DNA synthesis using short-lived tracers that carry minimal radiation burden.

Proliferation: Radiopharmaceuticals

[^{11}C] thymidine Work with tritiated thymidine *in vitro* led to the development of thymidine for PET imaging, labeled with ^{11}C in the methyl [38,39] and ring-2 positions [40,41]. Both tracers have been used successfully in patient studies. The difference in the labeling results in different profiles of *in vivo* labeled metabolites, as highlighted in Figure 1. Methyl-labeled thymidine generates a number of labeled acidic

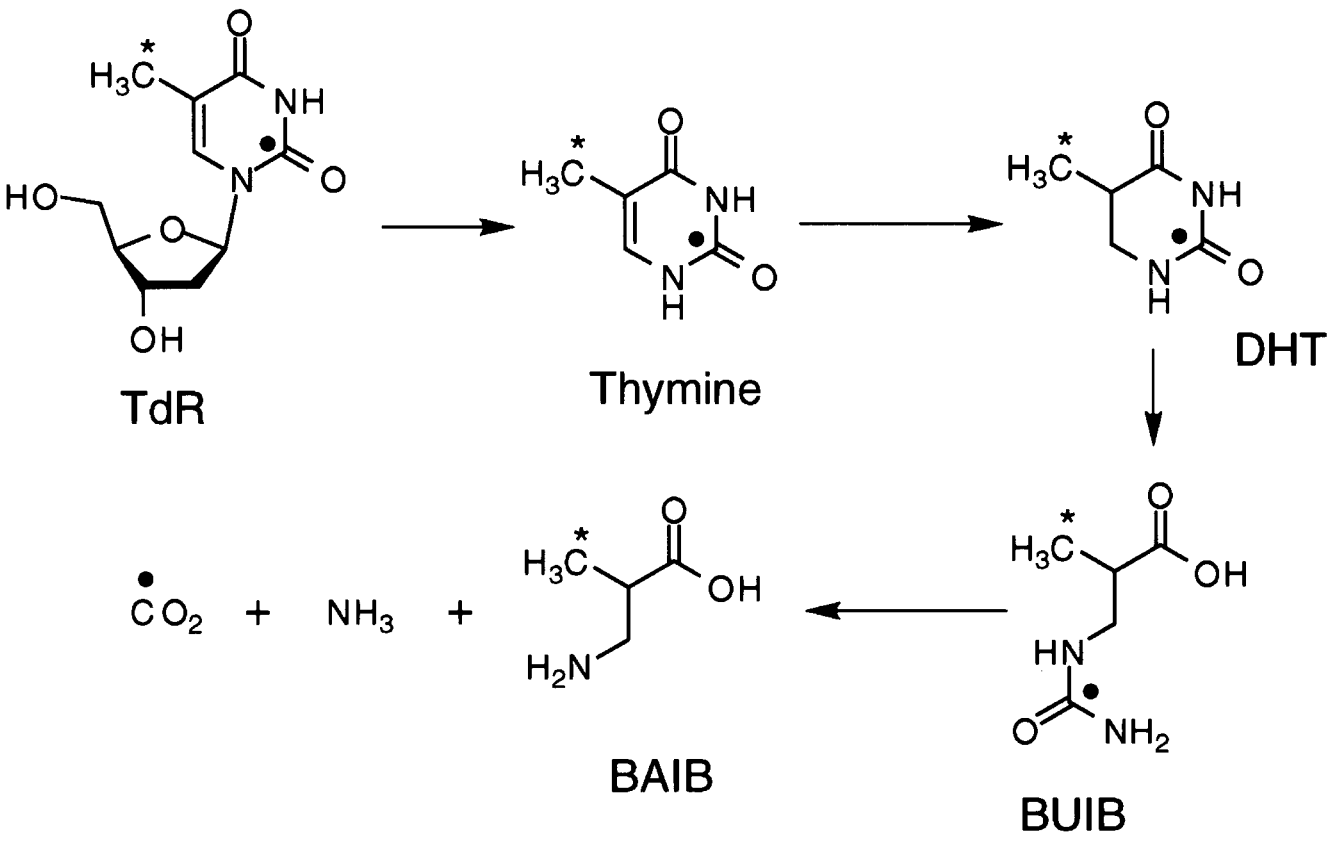

Figure 1. *Thymidine catabolism in vivo. The labeled species for ring-2 and methyl-labeled thymidine are indicated as follow: (●) Indicates labeled species for ring-2-labeled thymidine and (*) indicates labeled species for methyl-labeled thymidine. Abbreviations are as follows: TdR: thymidine, DHT: dihydrothymine, BUIB: β-ureidoisobutyric acid, BAIB: β-aminoisobutyric acid.*

metabolites [42,43]. The compounds typically have access only into tissues that also accumulate thymidine; therefore, they may not contribute to the image background to the same extent as more freely distributed labeled metabolites [43,44]. In contrast, the principal metabolite of 2-[^{11}C]thymidine, [^{11}C]CO_2, is readily transported into tissue and is therefore fairly ubiquitous [45,46]. It is, however, less likely to be trapped in tissue than the metabolites of the methyl-labeled compound [47–49] and therefore more confidently distinguished from thymidine incorporated into DNA in quantitative models of thymidine kinetics [50]. In either case, to fully interpret time–activity curves obtained after injection of [^{11}C]thymidine requires accounting for labeled metabolites.

Thymidine analogs The rapid catabolism of thymidine *in vivo* has two disadvantages: 1) Once metabolized, labeled thymidine is no longer available for incorporation into DNA, and thus only a fraction of the injected dose is used for measuring DNA synthesis. 2) Labeled metabolites confound image interpretation. In addition to these factors, the half-life of ^{11}C (20 minutes) is impractical for routine clinical imaging. These considerations prompted development of thymidine analogs for PET imaging (Figure 2). The analogs have fewer labeled metabolites and use longer-lived isotopes, but they are not components of normal DNA. Therefore, their uptake in tissue may not directly reflect the rate of thymidine precursor incorporation into DNA and may be influenced by factors other than cellular proliferation.

One strategy has been to develop analogs labeled with isotopes with a sufficiently long half-life to allow imaging after labeled metabolites are largely cleared from tissue. Two such tracers are IUdR labeled with ^{124}I (half-life=4.2 days) [51] and BUdR labeled with ^{76}Br (half-life=16 hours [52]). There is considerable experience with both IUdR and BUdR, which have been successfully applied to tumor growth measurements in a variety of applications [34]. Both are incorporated into DNA and retained in tissue, but they share the problem of rapid dehalogenation, which liberates the label as a free halide. As an imaging agent, there have been studies using IUdR labeled with a variety of iodine isotopes in both animals and patients [53–55]. The development of an [^{124}I]IUdR provides the opportunity for PET studies, with improved image quality and image quantification [51]. For both iodine- and bromine-based PET compounds, the relatively long half-life of the positron-emitting isotopes makes them attractive as compounds that can be shipped from a central production site; however, the longer lived tracers carry a higher radiation burden, leading to lower injected activity and poorer imaging statistics.

Several [^{18}F]-labeled analogs resistant to catabolism have been tested [56–59]. Most compounds were found to be inadequate cell proliferation tracers, either because much of activity was trapped in RNA rather than DNA or because they had insufficient concentration in proliferating tissues [60,61].

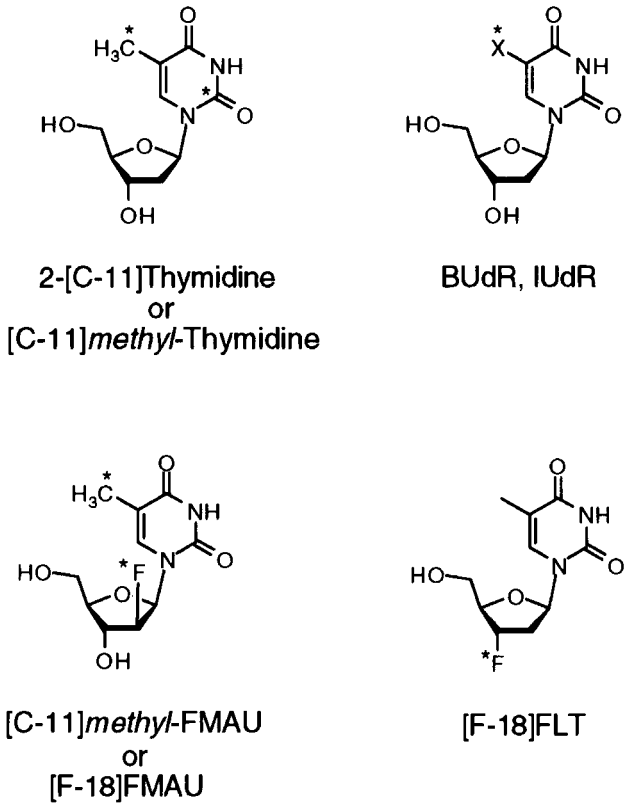

Figure 2. *Chemical structure of thymidine and labeled analogs IUdR/BudR, FMAU, and FLT (see text for full names). (*) Indicates sites that have been labeled with positron emitters. "X" in the IUdR/BUdR structure is iodine for IUdR and bromine for BUdR.*

Two thymidine analogs resistant to metabolism have shown promise as imaging agents in recent studies. FMAU [1-(2′-fluoro-2′-deoxy-β-D-ribofuranosyl)thymine] is an analog with a single fluorine substitution in the sugar [62]. It is phosphorylated by TK and is, to a variable extent, incorporated into DNA. It is stable to degradation; most of the tracer is cleared unchanged in the urine. Preliminary studies suggest its suitability for cell proliferation imaging [63,64], and further studies are underway to determine its utility in patients.

Another promising compound, [^{18}F]3′-deoxy-3′-fluorothymidine (FLT), is related to azidothymidine (AZT), which has important use in the therapy of HIV. FLT was also tested for the treatment of HIV, but toxicity limited its application as a therapeutic agent [65]. However, at tracer doses, toxicity is not an issue and, importantly, FLT can be labeled with the more convenient ^{18}F isotope, as opposed to AZT, which requires ^{11}C labeling for PET. FLT is taken up by cells and phosphorylated by TK at about 30% of the rate of thymidine [66]. It is resistant to degradation in dog blood and is excreted unchanged in the urine [67]. FLT acts as a chain terminator in DNA synthesis, so little is incorporated into DNA. However, its retention is dependent on the presence of TK, and thus it indirectly reflects cellular proliferation. [^{18}F]FLT imaging in dogs demonstrated high uptake in the marrow and tumors and low background activity outside of the kidneys and bladder.

Proliferation: Preclinical Studies and Image Analyis Considerations

Preclinical studies of [^{11}C]thymidine Several preclinical studies of [^{11}C]thymidine demonstrated its feasibility as a cellular proliferation imaging agent. Experiments in mice showed that intravenously injected thymidine had increased uptake in proliferative tissues that was independent of blood flow, despite thymidine's high first pass extraction from the blood [68–70]. Other studies established the nature of the species retained in tissues after thymidine injection and showed that retained label was in the form of labeled DNA and TTP, with little label in RNA [49,71]. Finally, several *in vitro* studies in treated cell lines compared the uptake of thymidine to tracers of energy metabolism such as deoxyglucose or FDG and to labeled amino acids [72,73]. These studies showed that, compared to energy metabolism and biosynthesis tracers, changes in labeled thymidine uptake more closely depicted changes in cellular growth.

General considerations for measuring cellular proliferation with labeled thymidine The goal of thymidine PET imaging is to measure regional *in vivo* cellular proliferation. In addition to answering the qualitative question, "Is the tumor growing or not?" PET offers the capability of providing quantitative regional estimates of proliferation. Because multiplying cells must generate DNA for cell division, the synthetic rate of DNA (SR_{DNA}, μmol DNA/min per gram tissue) is a quantitative measure of proliferation. The approach to using thymidine to estimate SR_{DNA} is based on the four-factor model of Cleaver [35]. In this model, thymidine nucleotides arising from *de novo* synthesis (endogenous pathway) and from the exogenous pathway freely mix in the phosphorylated nucleotide (DNA precursor) pool (see Figure 3). Unless there is a shortage of DNA precursors, the rate of DNA synthesis depends on the "proliferative state" of the tissue and not on the concentration of precursors. In equilibrium, the total biochemical flux of nucleotides through the nucleotide precursor pool and into DNA equals the rate of DNA synthesis. Therefore, assuming that half the nucleotide base pairs contain thymidine [50],

$$SR_{DNA} = 2 \cdot \frac{1}{f_{ext}} \cdot Flux_{TdR} \quad (1)$$

where $Flux_{TdR}$ is the total flux of thymidine nucleotides from the precursor pool into DNA (units μmol/min per gram). The term, f_{ext}, reflects the fact that intravenously injected labeled thymidine follows the exogenous pathway and therefore estimates only a fraction of total thymidine flux and corrects

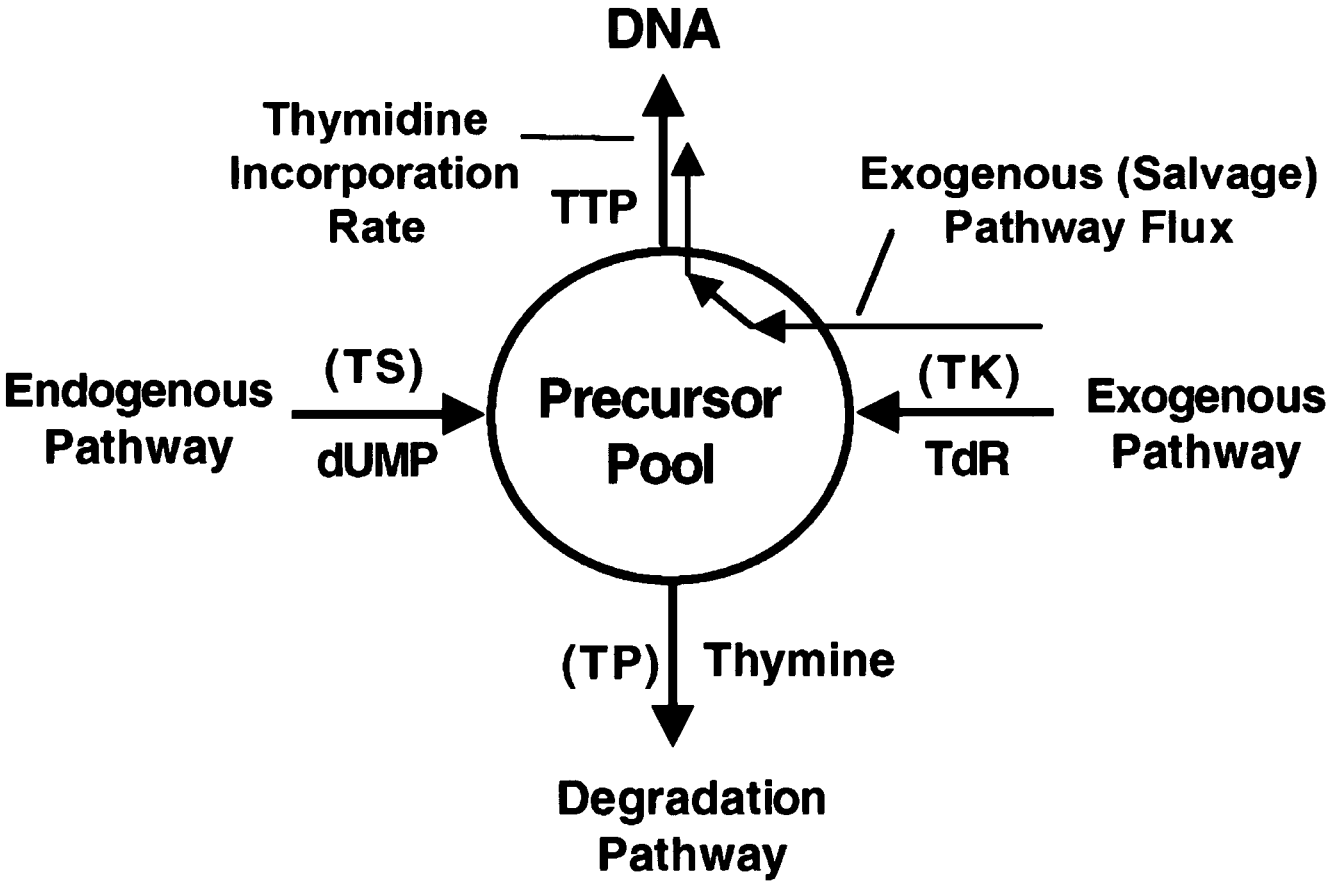

Figure 3. *Four-factor model of thymidine utilization (adapted from Ref. [35]). The chemical species entering and leaving the precursor pool are shown. Abbreviations in parentheses refer to enzymes at control points in the model: TS: thymidylate synthetase; TP: thymidine phosphorylase; TK: thymidine kinase. The line following the exogenous pathway into DNA indicates exogenous thymidine flux measured by labeled thymidine.*

for thymidine arising from the endogenous pathway. Early studies of the exogenous versus the endogenous thymidine pathways indicated that the two might be handled independently by the cell and have different intracellular pools [74]. Subsequent work, however, demonstrated that both endogenous and exogenous thymidine freely mix within the cell and that relative utilization could be predicted based on the level of extracellular thymidine [75].

Quantitative analysis of [^{11}C]thymidine images The least complex approach to image quantitation uses static uptake measures such as the standardized uptake value or SUV:

$$SUV = \frac{A}{(ID/weight)} \quad (2)$$

where A is the average tissue activity (μCi/g), ID is the injected dose of tracer (mCi), and weight is the patient weight (kilograms). Although SUV is simple to calculate, it leads to significant bias in estimating thymidine flux into DNA because it fails to consider the time course of imaging and does not account for labeled metabolites. Several kinetic models have been formulated to address these issues [44,50,76,77]. Using time–activity curves obtained from blood sampling as input data to the model, kinetic parameters can be estimated by optimizing the fit of the model to the observed time course of tissue uptake measured by dynamic PET imaging.

Because the imaging device measures the total regional radioactivity concentration and cannot distinguish individual radiochemical species, labeled metabolites arising from the parent compound can affect quantitative interpretation of labeled thymidine, which is rapidly catabolized *in vivo*. Correction for labeled metabolites can be handled in several ways. In tumor imaging the approach of subtracting the metabolite background estimated from a reference tissue does not work because there is no tissue with properties similar enough to be valid. To overcome this, Mankoff *et al.* [50] proposed a detailed model accounting for both thymidine and metabolites using data obtained from blood analysis as input to the model. Animal studies validated this model's ability to predict the time course of [^{11}C]thymidine incorporation into DNA, and simulations and animal studies suggested that this analysis provided reliable values for thymidine flux [78]. Alternate simplified methods can provide estimates of thymidine flux into or retention in DNA [79–82] but do not provide detailed kinetic insights.

Kinetic analyses are usually applied to time–activity curves obtained by region-of-interest (ROI) analysis of the dynamic images, but recently developed methods provide pixel-by-pixel images of physiologic parameters, such as thymidine flux into DNA. The graphical method and spectral analysis are both attractive for pixel-by-pixel parameter estimation because of their computational efficiency [83]. Another approach, mixture analysis, separates each pixel of dynamic image data in to a small set of characteristic time–activity curves and is attractive in that it retains the power of compartmental analysis with computational efficiency suitable for pixel-by-pixel analysis [84]. Pixel-by-pixel methods are likely to be important for compounds such as [^{11}C]thymidine, where simple summed images provide a biased picture of cell proliferation, due to radioactivity not incorporated into DNA.

Brain tumor imaging Because the intact blood–brain barrier limits the transport of thymidine in the brain, imaging the cellular proliferation of brain tumors requires special consideration. Eary *et al.* [85] showed that thymidine provided unique information for brain tumors, but the interpretation of static thymidine images was confounded by the blood–brain barrier (BBB) breakdown that frequently accompanies brain tumors and their treatment. In somatic tissues, thymidine and metabolites have similar rates of transport [78], but in the brain the [^{11}C]CO_2 metabolite has higher rates of transport across the BBB than thymidine [86]. Preliminary results using a separate [^{11}C]CO_2 study to independently measure metabolite kinetics [85] showed that compartmental analysis can correct for the metabolite background in the brain and thereby separate the effects of transport across a damaged BBB versus retention by DNA incorporation in the tumor.

Proliferation: Clinical Studies

IUdR and BUdR The initial studies of cellular proliferation imaging in patients used IUdR and BUdR [87], but dehalogenation produced a high background, and they did not find regular clinical use. In a more recent study using planar imaging of [^{131}I]IUdR, about 50% of tumors showed tracer localization [88]. The simplest way to overcome the problem of free halogen is by imaging 24 to 48 hours after injection [54], which allows for clearance of much of the free iodide. In a study of patients with brain tumors imaged with [^{131}I]IUdR and SPECT, Tjuvajev *et al.* [54] showed that 2 hours after injection, uptake around the tumor site was similar to that seen on the contrast enhanced MRI and was consistent with BBB breakdown. However, when patients were re-imaged at 24 hours, the level of activity in the tumors went down and the pattern of localization changed to the periphery of the tumor, consistent with active tumor. Ongoing studies are investigating IUdR labeled with ^{124}I, a positron emitter that offers the possibility of significant refinements in image quality and quantitative analysis [51].

[^{11}C]thymidine Labeled thymidine has been employed in imaging trials utilizing both the methyl- and ring-2-labeled compounds. The initial trials with the methyl-labeled compound studied 10 patients with non-Hodgkin's lymphoma [76]. Uptake tended to be higher in those with more aggressive histologies. In another study of nine patients with squamous cell head and neck cancer, the tumors were visible in all patients [77]. They also studied three patients with higher-grade tumors, including non-Hodgkin's lymphoma and neuroendocrine tumors, and found higher uptake than in the other tumors. Increased activity was also seen in the liver, kidney, and heart wall. This group subsequently worked on a compartmental model to assist in quantifying

thymidine uptake and found that taking blood pool activity into account was necessary [89]. They also extended their work to cerebral neoplasms, where [^{11}C]thymidine was able to visualize most brain tumors [90].

Ring-2-labeled thymidine has been used in brain tumors, sarcomas, and lung cancers [85,91,92]. In the initial studies by Vander Borght [92], PET thymidine imaging identified 11 of 14 untreated brain tumors with an average uptake approximately twice that of normal brain. No correlation was seen between tumor grade and thymidine uptake. This was primarily driven by the high uptake seen in four patients with low-grade meningiomas. In most cases, better contrast was seen between the tumor and normal cortex with thymidine than FDG, because of the high uptake of FDG in the normal brain. Eary *et al*. [85] compared PET imaging with ring-2 thymidine, FDG, and MRI in 13 patients. Although nearly equal number of tumors were visualized with each technique, distinct differences could be seen in individual patients. The thymidine scans showed different uptake patterns compared to the other studies in about half of the patients, indicating that different information was being obtained. The expectation was that images of proliferation would more closely match the clinical progression, and was seen with some, but not all, cases. Part of the discrepancy was thought to result from label accumulation associated with BBB disruption. Preliminary application of a kinetic model to brain tumor showed promising results and suggested an improved ability to delineate active tumor from treatment effects (see Figure 4).

Ring-2-labeled thymidine has also been used to image high-grade sarcomas and small-cell lung cancer and to monitor their response to chemotherapy [91]. In four patients with successful treatment, the fractional decline in thymidine retention was greater than with FDG. Thymidine SUV declined by an average of 64%, the thymidine flux constant declined a mean of 84% (see Figure 5). This pilot study indicates that thymidine may be of particular use in measuring early response to therapy.

2-[^{11}C]thymidine has also been used to guide the application of new anti-cancer agents, both to assess response and to provide information on mechanisms of action [27,82]. For example, thymidine imaging was used in a preliminary study of patients receiving a thymidylate synthetase (TS) inhibitor, which would be expected to increase the utilization of the salvage (exogenous) thymidine pathway for DNA synthesis. Images showed increased

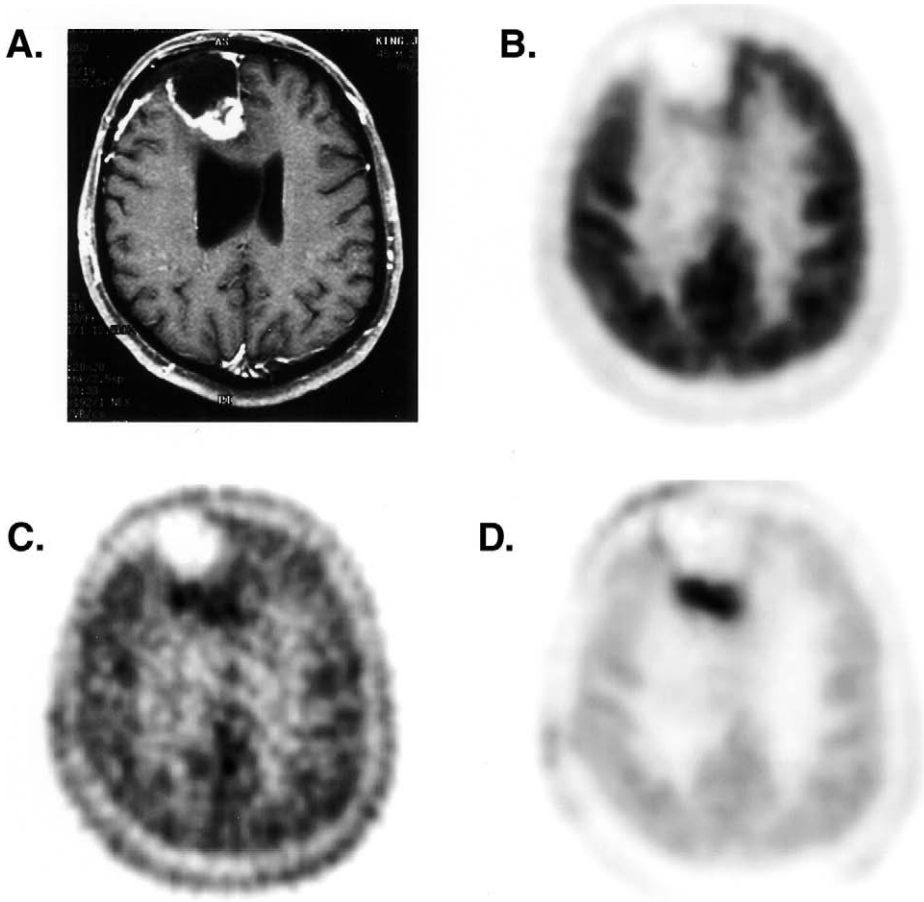

Figure 4. *Images of a patient with a high-grade glioma status post surgery, chemotherapy, and radiotherapy with a clinical suspicion of recurrent tumor on MRI imaging. (A) Contrast-enhanced T1-weighted MRI, (B) summed FDG image, (C) summed [^{11}C]thymidine image, (D) thymidine flux image obtained using compartmental model and mixture analysis. The thymidine flux image, which corrects for labeled metabolites and unincorporated tracer, most clearly delineates the tumor. The patient's subsequent clinical course was consistent with recurrent tumor.*

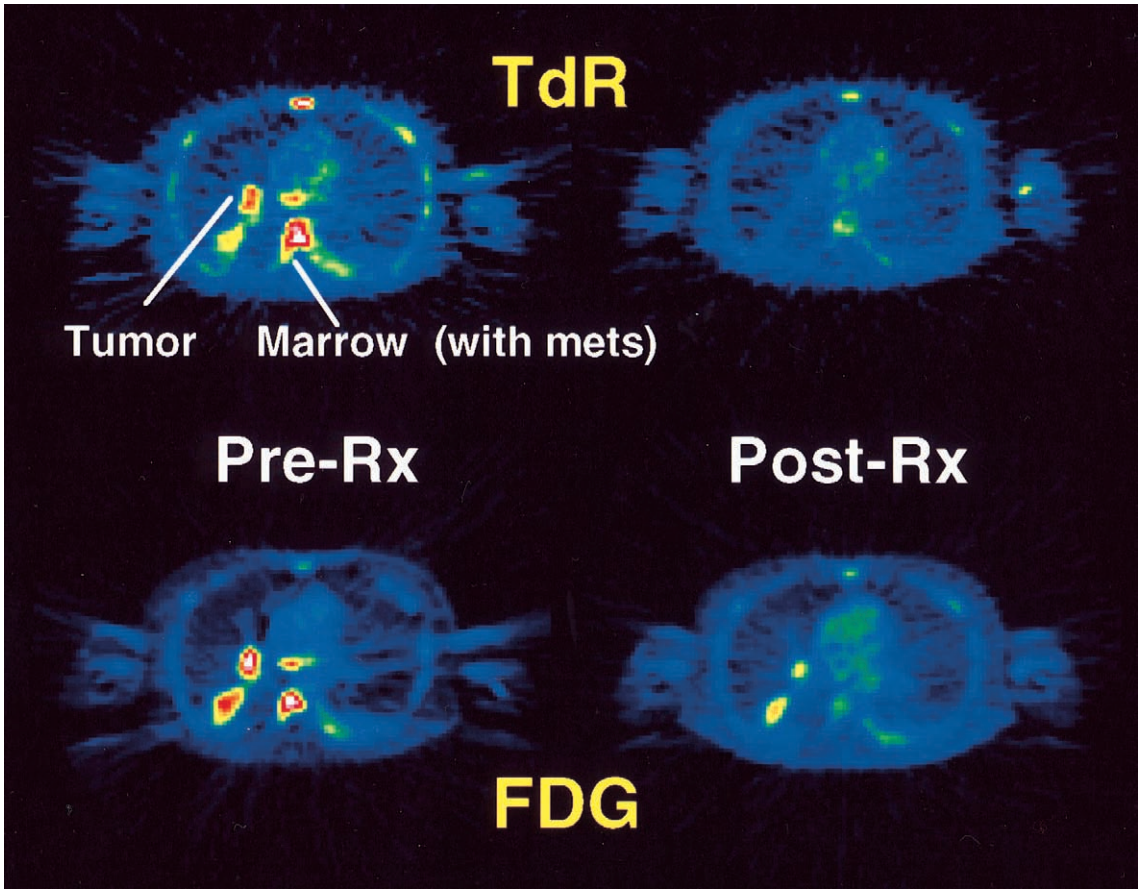

Figure 5. *Images from a patient imaged before and after one cycle of chemotherapy for small-cell lung cancer. Images on the left show pre-therapy summed FDG and thymidine images; images on the right are summed images after one week of therapy. Images show the lung tumor and vertebral bone marrow metastases. Although both tracers indicate a decline in tracer uptake in response to therapy, the decline is much greater in the thymidine images, even without metabolite subtraction. The patient went on to have a complete clinical response after several more cycles of chemotherapy.*

thymidine retention in tumors after the administration of the TS-inhibiting drug compared to pre-drug uptake [82].

Thymidine analogs other than IUdR and BUdR Recent patient studies have been conducted with FLT [67]. Similar to the results in dogs, studies in patients have shown superior tumor to background activity with SUV levels in the range of 2–7. Normal bone marrow, a rapidly proliferating tissue, also demonstrated high uptake (SUV 4–6). Low background was seen in the normal brain, muscle, heart, lungs, and most other organs. Increased activity was seen in bowel (SUV 2–3) and in the kidney, resulting from excretion. Unlike the dog, significant FLT accumulation was found in the normal liver in humans. FLT appears to be a promising agent to measure tumor proliferation, but further validation is needed.

Proliferation: Summary

Cell proliferation imaging is based on extensive data obtained from laboratory investigation of labeled thymidine. [^{11}C]thymidine, labeled in the ring-2 or methyl position, is the natural extension of earlier work using tritiated thymidine. Proliferation imaging using [^{11}C]thymidine requires consideration of labeled metabolites; however, quantitative approaches can provide reliable estimates of cellular proliferation by measuring thymidine flux from the blood into DNA in tumors. [^{18}F]-labeled thymidine analogs that are resistant to catabolism *in vivo*, such as [^{18}F]FLT and [^{18}F]FMAU, may simplify quantitative analysis and may be more suitable for clinical studies, but will require careful validation to determine how their uptake is quantitatively related to cell growth. Early clinical studies, mostly using [^{11}C]thymidine, have demonstrated the power of cellular proliferation imaging to characterize tumors and monitor response early in the course of therapy. Patient imaging using the PET thymidine analogs is at an earlier stage but appears promising as a clinically feasible approach to cellular proliferation imaging.

Tumor Receptor Imaging

Tumor Receptors: Biology and Biochemistry

Proliferation of some types of cancer is regulated by hormones that bind to membrane and intracellular receptors. The hormone–receptor complex activates signal transduc-

tion pathways that are important in controlling transcription and cell growth. Tumor receptors can be targeted by hormones for treatment of these tumors. Drugs based on hormone antagonists or agonists have been successfully used in regulating growth of breast and prostate cancers [93,94]. The presence of tumor receptors provides a mechanism for selective uptake of radiolabeled hormones as tumor imaging agents. Receptor-based imaging can provide information about the location of the tumor and assess the level and functional status of the receptor. Determination of the presence or absence of receptors in tumors can be important in directing therapy. Particularly in the case of advanced disease, where within-site or site-to-site heterogeneity of receptor expression can occur, imaging methods to assess regional receptor expression can offer significant advantages over biopsy-based methods in directing therapy.

Hormone receptors and breast cancer Approximately two-thirds of breast cancers are hormone sensitive, and it has been established that ER and PR status are indicators of prognosis [2]. Estrogen-receptor-positive (ER+) cancers have a more favorable prognosis than do estrogen-receptor-negative (ER−) cancers. Tumors that are both ER+ and progesterone-receptor-positive (PR+) have the best prognosis. In addition, the ER and PR status of the breast cancer determines the likelihood of response to hormonal therapy [5], and thus directs the choice of systemic therapy. It is best to assess the receptor concentration of the primary tumor at initial diagnosis. Knowledge of the receptor status of the metastatic or recurrent disease is also important in selection of subsequent systemic treatment. The receptor status of the metastatic or recurrent disease may be different than the receptor status of the primary tumor. A discordance rate of 3% to 35% in ER status between primary tumors and their metastases, as well as between different metastases from the same tumor, has been reported [7,8,95]. This difference is considered clinically significant and may account for the lack of response to hormonal therapy of some patients with presumably ER+ tumors.

In vitro receptor assays Currently, the ER and PR status of breast cancer are routinely assessed by *in vitro* assays of biopsy tissue. These assays, however, have limited ability to assess the functional status of the receptors and to predict tumor responsiveness to hormone therapy. Only 55% to 60% of patients with ER+ cancers respond to hormonal therapy; conversely, 8% to 10% of patients with ER− cancers respond [5]. The conventional *in vitro* radioligand competitive binding assays used to assay for ER, require fresh or fresh-frozen tumor specimens of adequate size and tumor cellularity, because the receptor distribution within a given tumor is very heterogeneous [95,96]. This technique cannot be used to measure receptor content on bodily fluids or bone specimens, and, furthermore, false-negative results can occur with high levels of competing estrogens in the blood in patients undergoing hormone therapy. Newer immunohistochemical techniques are less dependent on the sample size, can identify receptors in bodily fluids and bone, and give results that are independent of exogenous hormone used by the patient. However, immunohistochemical techniques are limited in that the receptor may be detected even if the ER is nonfunctioning [97]. Both techniques suffer from interlaboratory variability. A better method for functional assessment of receptors is critically needed to reliably identify patients likely to benefit from hormonal therapy. This is especially true in clinical scenarios where the sampling error from biopsy is likely to be a problem, such as patients with large tumors or multiple sites of disease.

Hormone receptors and prostate cancer The majority of prostate cancers express androgen receptor (AR). The presence of AR in tumor may predict the patient's responsiveness to hormonal therapy with estrogens, androgen antagonists, inhibitors of androgen biosynthesis, or castration [98,99]. However, the correlation between AR positivity and response to hormonal therapy in prostate cancer is not as good as that between ER and PR positivity and response to hormonal therapy in breast cancer [98–100]. This may be related to the heterogeneity of prostate cancer with respect to AR localization [101]. Most prostate cancers that initially respond to hormonal therapy eventually become hormone independent [94,102,103]. The use of an AR-based imaging agent to assess AR function may provide a better representation of AR status in prostate cancer and may help to understand some of the mechanisms responsible for resistance to hormonal therapy.

Why PET imaging of hormone receptors? In vivo measurement of the receptor content of breast and prostate cancers could offer several advantages over current *in vitro* methods. These include assessing the receptor status of the entire tumor volume rather than just a part of the tumor (addressing the intrinsic heterogeneity of receptor expression), assessing the biologic availability of the receptors *in vivo*; and evaluating the effects of therapy on the receptor content of the tumor. In addition, *in vivo* imaging can simultaneously assess the receptor status of the primary and metastatic lesions, many of which may be inaccessible to biopsy. PET's ability to image ligand binding quantitatively at tracer concentrations well below typical blood steroid concentrations provides a distinct advantage over other imaging modalities, such as SPECT [15]. This has encouraged considerable efforts to develop steroid-based imaging agents, especially estrogenic radiopharmaceuticals.

Tumor Receptors: Radiopharmaceuticals

Several radiolabeled estrogenic compounds have been developed, including agents for conventional scintigraphy and for PET. This review will focus on positron-emitting radioligands.

Requirements for steroid-based radioligands Requirements for successful design of a steroid-based imaging agent

include high binding affinity for the receptor, high target to nontarget selectivity, high specific activity, and appropriate *in vivo* metabolism and clearance. Katzenellenbogen and colleagues demonstrated that the ratio of receptor binding affinity to nonspecific binding was an important predictor of *in vivo* uptake efficiency and selectivity of the ligand [104–109]. Ligands with ratios close to those of the natural hormones are preferred. *In vivo* selectivity is measured by the radiotracer uptake in the target tissue compared with nontarget tissues. In addition, the uptake should be selectively displaced from the target tissues. The specific activity of the ligand is important because the receptors are saturable and have limited uptake capacity. Specific activity of at least 1000 Ci/mmol [110,111] is needed for successful imaging of steroid receptors with PET. A suitable radioligand should have slow *in vivo* metabolism to allow adequate uptake by the target tissue. Recently, it has been recognized that the uptake of steroid ligands in the target tissue can be improved if the ligand has high affinity for the sex-hormone-binding globulin (SHBG or SBP) [112,113], a serum glycoprotein that acts as a transporter for steroid hormones, facilitating uptake into receptor-positive cells and providing protection from metabolism [113–116].

Estrogen-receptor-based imaging compounds Several halogenated derivatives of estrogens, estradiol (steroidal) and hexestrol (nonsteroidal), have been developed and evaluated as ER-based radiopharmaceuticals for imaging breast cancer [104,105,117,118]. The nature of halogen label and its site of substitution affect receptor binding affinity and nonspecific binding (see Figure 6). When a large halide, such as bromine and iodine, is positioned on the A-ring of either estradiol or hexestrol [119], the resulting ligands have poor selectivity and unfavorable *in vivo* distribution. Conversely, when a large halogen is substituted at the 16α position of estrogen, it results in selectivity similar to the natural hormones and a favorable *in vivo* distribution [100,118,120].

The use of ^{18}F has several advantages. Fluorine is a smaller halogen and can substitute many positions of the estrogen molecule without significantly changing binding. The half-life is long enough to allow for multistep synthesis of ligands as well as uptake into the target tissue with clearance from nontarget tissues during imaging. Several ^{18}F-labeled estrogens with high specific activity have been synthesized and evaluated in animals [121–123]. The most promising, 16α-[^{18}F]fluoroestradiol-17β (FES) can be prepared with high specific activity, generally greater than 1000 Ci/mmol, in 90 minutes with an automated procedure [122–126].

Since the development of FES, other compounds have been developed and tested [104,127], but none have demonstrated significant advantages over FES. One compound, [^{18}F]moxesterol, was superior to FES in *in vitro* testing and *in vivo* studies in rats, but showed poor uptake in patients [128]. This disappointing result may be due to poor binding to SBHG. Poor SBHG binding would not affect studies performed *in vitro*, and rodents do not have SBHG.

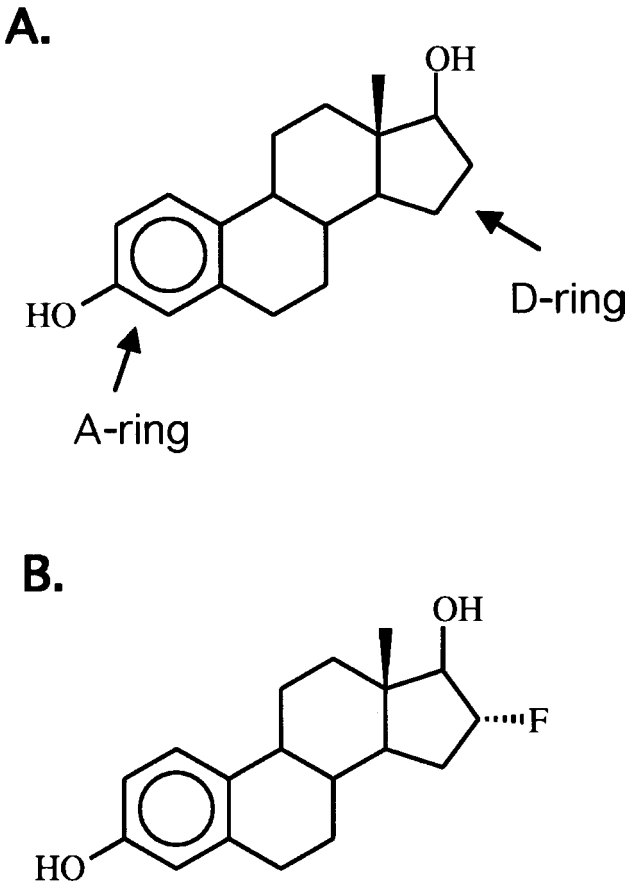

Figure 6. *Chemical structure of estradiol (A) and FES (B). Ring positions described in text are noted.*

However, lack of SBHG binding would adversely effect patient imaging. Estradiol analogs with improved SBHG binding are being developed and tested.

In addition to ER imaging compounds related to estradiol, an analog of tamoxifen labeled with ^{18}F has been developed as a tracer to assess tumor ER status and responsiveness to tamoxifen therapy [129,130]. Limited studies of this compound in patients with breast cancer demonstrated low specific binding to ERs and high nonspecific binding in other tissues [130].

Progesterone-receptor-based imaging compounds Several radiolabeled progesterone analogs have been developed for imaging by PET [131–133]. One of these, 21-[^{18}F]fluoro-16α-ethyl-19-norprogesterone (FENP), an analog of the potent progesterone, ORG 2058, has been made with high specific activity and has high affinity for PRs (60 times that of progesterone), and receptor-mediated uptake in target tissue in rats [131,134]. FENP had favorable *in vitro* and *in vivo* characteristics in preclinical testing; however, imaging results in patients with breast cancer were disappointing due to low target-to-background uptake ratio, poor correlation of tumor uptake with PR content, and high nonspecific uptake [104,135,136]. The difference between the preclinical and the clinical results was most likely to be due to differences in metabolism between

rats and humans. The search for a optimal progesterone-based imaging compound continues.

Androgen-receptor-based imaging compounds Several ^{18}F-labeled androgens have been developed as potential imaging agents for prostate cancer. The most promising of these has been 16β-[^{18}F]fluoro-5α-dihydrotestosterone (FDHT), a fluorinated analog of the naturally occurring male sex hormone dihydrotestosterone. FDHT has been synthesized with adequately high effective specific activity [137]. Studies in male rats treated with diethylstilbestrol to suppress *in vivo* biosynthesis of androgen and therefore increase concentration of unoccupied ARs demonstrated high selective uptake of FDHT in the prostate, with a mean prostate-to-muscle ratio of 25 at 4 hours after administration of the tracer [137]. In addition, FDHT showed high affinity for SHBG. Studies in male baboons demonstrated high FDHT uptake in the prostate that was blocked with administration of testosterone, indicating AR-mediated binding [138]. Preliminary studies with FDHT in patients with prostate cancer have been less successful due to relatively low uptake in the prostate cancer and high activity in the normal organs in the abdomen and pelvis (unpublished data). Further patient studies and the development of other AR imaging compounds may be able to overcome these limitations and provide a method for quantifying AR expression in prostate cancer.

Tumor receptors: Preclinical Studies and Image Analysis Considerations

Preclinical studies of FES in animals Studies in immature female rats demonstrated high uptake of FES in ER-rich uterus compared with nontarget tissues, giving average uterus-to-blood ratios exceeding 80:1 at 2 hours [122]. In addition, target tissue uptake was blocked by coadministration of estradiol. To investigate the relationship between FES uptake and ER content of mammary tumors, FES was evaluated in mammary tumors in rats [139]. The metabolism of FES was rapid and most of the activity in blood and nontarget tissue resulted from metabolites; however, the target tissue (uterus and tumor) activity was mainly unmetabolized FES. No correlation was found between ER content of the tumor and tumor uptake of FES at 3 hours after administration, even after normalizing for differences in blood flow [139]. This study suggested that quantitative estimates of tumor ER content would require a complex pharmacokinetic model involving ligand uptake, retention and washout from target and nontarget tissues. Nevertheless, preliminary studies of FES in patients showed an

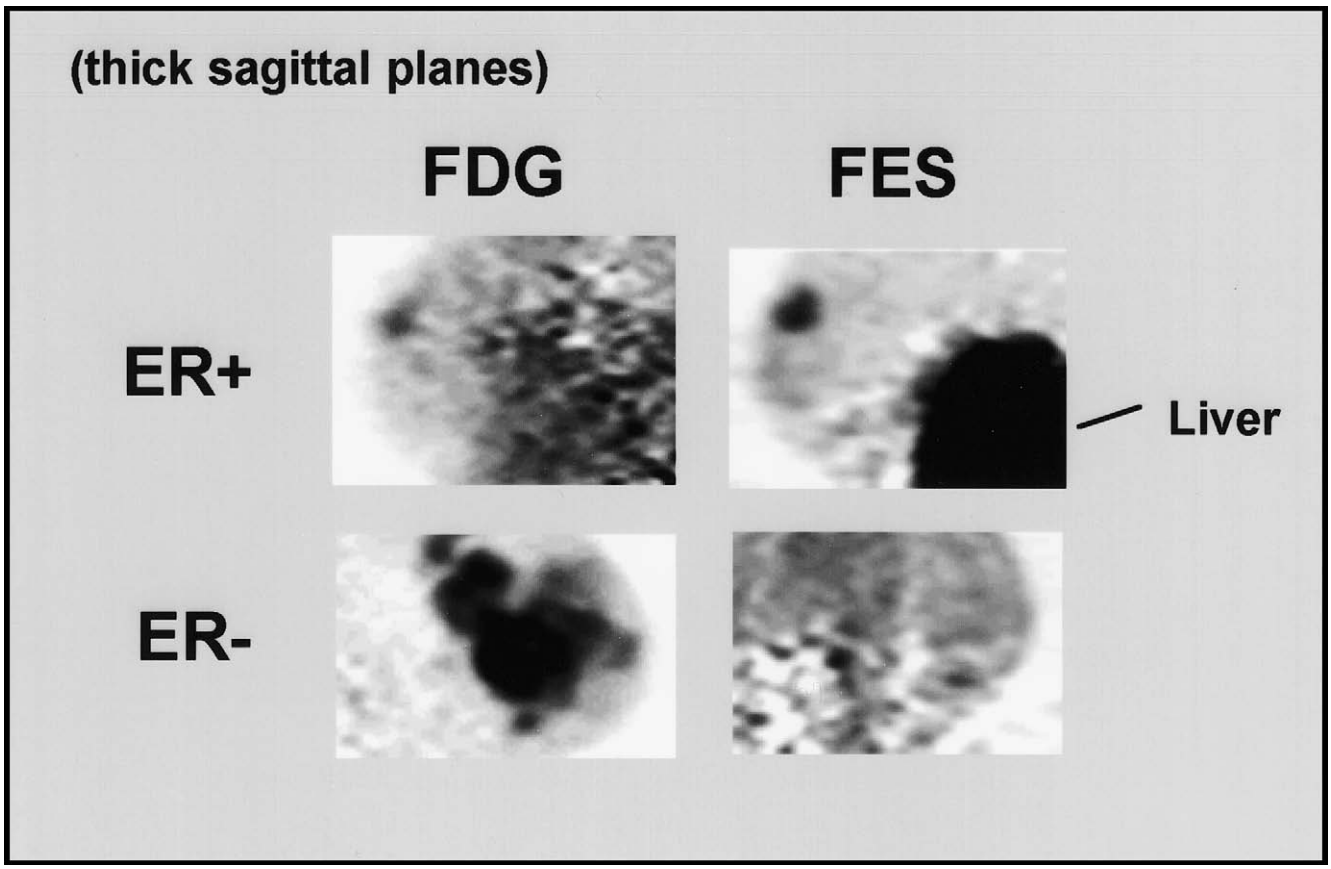

Figure 7. *Images of ER expression in breast cancer. Thick sagittal images, similar in orientation to medial–lateral oblique (MLO) mammograms, are shown for two patients imaged with FDG (left) and FES (right). The patient on the top had an ER-positive right breast tumor faintly seen on FDG images and clearly seen on FES images. Uptake in the liver, the site of steroid metabolism, is also seen on FES images. The patient on the bottom had an extensive ER-negative cancer in the left breast. Despite markedly abnormal uptake on the FDG image, no significant FES accumulation is seen.*

excellent correlation between tracer uptake and *in vitro* radioligand assays of ER content [140]. Subsequent analyses have suggested that uptake of labeled estrogens correlates with receptor expression in tissues with intermediate levels of expression, such as breast cancers, but not necessarily in tissues with higher levels of expression, such as the uterus [141].

Approaches to image analysis A precise model for quantifying ER content from FES imaging has been elusive. This is not surprising in view of the complexity of estrogen metabolism and transport, as noted above. Furthermore, the likelihood that SHBG significantly affects transport makes many animal studies, including rodent models, inadequate for studying tracer kinetics. Recent data from patient studies [142] confirmed that FES is rapidly metabolized to glucuronide and sulfate conjugates, metabolites which would not be expected to have access to the intracellular space and would be unlikely to bind to ER. If metabolites are not trapped, quantitative analysis of FES images might be improved by relatively simple metabolite subtraction approaches, such as the graphical method described above for thymidine image analysis [80]. An alternate graphical approach proposed by Moresco *et al.* [143] is based on the same principle, but estimates FES distribution volume rather than flux. This approach was used to estimate ER expression in meningiomas using FES-PET, and showed some degree of correlation to *in vitro* ER estimates. Further testing is needed to understand the influence of labeled metabolites in patient studies, including whether or not metabolites are trapped in ER-containing tissues, and whether approaches to account for metabolites improve the estimation of tissue ER content.

Recent patient studies directly measured FES binding to SHBG and showed that 40% to 70% of circulating FES is bound to SHBG [144], supporting the concept that SBHG binding is important. The extent of binding to SHBG depended on the concentration of SHBG in the blood. It may therefore be necessary to account for the influence of SBHG concentration on tracer uptake in devising approaches to quantitative analysis. The use of primate models or recently developed transgeneic rodent models which express SHBG [145] may shed further light on how SBHG affects the quantitative uptake of FES and other estrogen analogs in ER tumors.

In the absence of a model for image quantification, investigators have relied on simple uptake measures, such as the SUV (Equation 1), to quantify tracer uptake. To allow for clearance of metabolites and unbound tracer, measurement of uptake typically starts 90 minutes after tracer injection [146], although earlier imaging times may be feasible [142]. Simple uptake measures have shown a high degree of correlation with *in vitro* measures of ER content

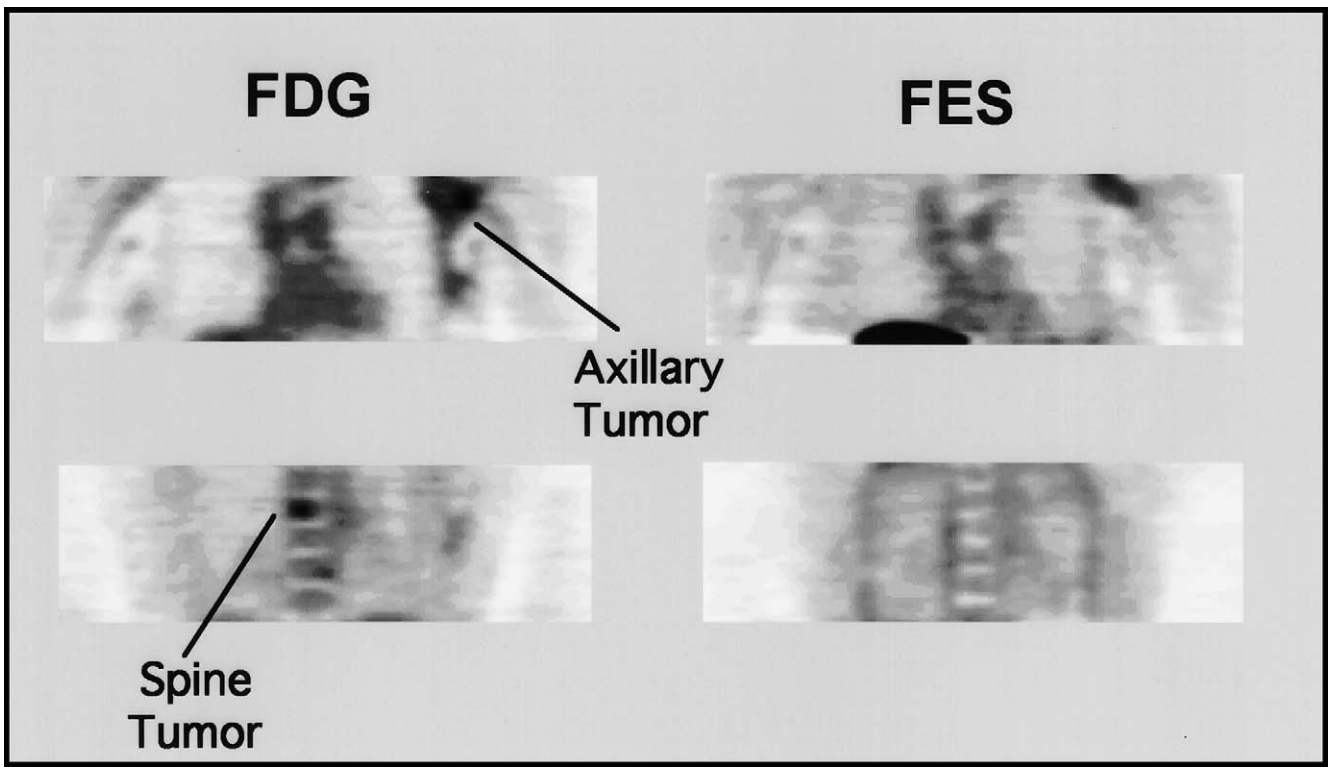

Figure 8. *Heterogeneous ER expression demonstrated by PET imaging. Coronal images of FDG (left) and FES (right) are shown for a patient with an extensive breast cancer involving the left axillary tail of the breast and much of the left axilla. The tumor was ER-positive by a limited biopsy of the axillary portion of the tumor. FES imaging shows uptake in only a portion of the axillary tumor and no accumulation in a spinal metastasis seen on FDG imaging and confirmed by bone scan, suggesting an ER-negative metastasis. On clinical follow-up after chemohormonal therapy, the axillary lesion resolved; however, the patient experienced widespread progression of her bony disease. Follow-up FDG and FES imaging (not shown) again demonstrated that the bony metastases did not bind estrogen, as had been the case on initial imaging studies.*

[140], and a recent study of FES uptake as a predictor of response of hormonal therapy [147] showed a good correlation between pre-therapy FES uptake and response to tamoxifen, discussed in more detail below.

Tumor Receptors: Clinical Studies

Based on the promising results in preclinical studies, FES has been evaluated in humans as an agent for receptor imaging of breast cancer (see examples in Figure 7). The first human study of FES-PET was performed on 12 postmenopausal women with primary breast cancer. Mintun *et al.* [140] found a good correlation between the tumor FES uptake measured on PET images (expressed as the percentage of injected dose per milliliter) and the ER concentration of the tumor determined by conventional quantitative ligand binding assays of the tumor tissue (r=0.96, P<.001). This human study suggested that FES uptake could be used to assess ER content of the tumor noninvasively. In a subsequent study of 16 patients with ER+ metastatic breast cancer, FES-PET identified 53 of 57 (sensitivity 93%) hormone-sensitive metastatic foci [148]. In addition, following initiation of anti-estrogen therapy, tumor uptake of FES decreased, further confirming that the tumor uptake of FES is a receptor-mediated process, and suggesting that FES-PET could be used to evaluate the availability of functional ERs in breast cancer to predict the likelihood of response to anti-estrogen therapy.

To extend these results, tumor uptake of FES was compared with *in vitro* ER levels and tumor uptake of FDG in 43 patients with untreated advanced breast cancer [146]. The results of FES-PET correlated well with *in vitro* ER assays, with an overall agreement of 88%, similar to that observed with replicate *in vitro* assays. However, there was no significant relationship between tumor FDG uptake and either FES uptake or the ER status. These results indicated that, although ER+ tumors are expected to be less aggressive than ER− tumors, the ER status of breast cancer cannot be predicted by measuring FDG uptake as a surrogate measure of tumor aggressiveness. In the same group of patients, to assess tumor heterogeneity and within-patient ER concordance between primary and metastatic foci, 50 tumor sites in 17 patients were evaluated with FES-PET [149]. Complete concordance among multiple lesions within a patient was observed in only 76% of patients. The level of concordance observed by FES-PET is comparable to that found by *in vitro* ER assays when multiple sites have been biopsied. (See Figure 8 for an example of heterogeneous ER expression.) This study also showed that patients with FES+ disease had longer median survival than did patients with FES− breast cancer [149]. These results are consistent with earlier observations that patients with ER+

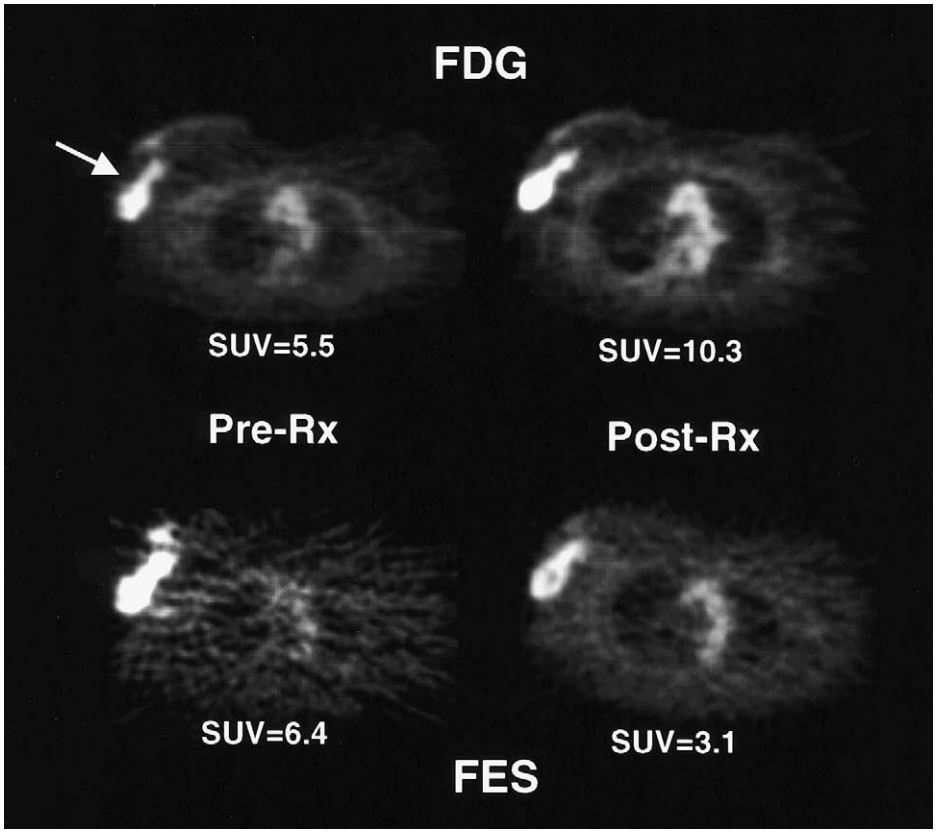

Figure 9. *"Metabolic flare" after the initiation of tamoxifen therapy. Transaxial images of a patient with a right locally advanced breast cancer taken before and one week after tamoxifen treatment. Images show an increase in FDG uptake as a manifestation of increased energy metabolism after the start of treatment. In addition, the high level of FES uptake pre-therapy and a decline after the start of therapy suggests an appropriate biologic basis for anti-estrogen therapy. The patient went on to have a response to tamoxifen. SUV refers to standardized uptake value (see text for details).*

breast cancer have a longer overall survival than do patients with ER− disease, independent of the stage of disease.

Patients with hormone-sensitive (ER+ and/or PR+) advanced breast cancer are candidates for antiestrogen therapy. Shortly following institution of treatment, 5% to 20% of these patients experience a phenomenon known as the hormonal "flare" reaction, characterized by increased pain in the sites of osseous metastatic disease and pain and erythema in soft tissue lesions [150]. Affected patients may develop hypercalcemia and may show what appears to be disease progression on bone scintigraphy [150–152]. Clinically, it is sometimes difficult to distinguish a flare reaction from disease progression. The clinical flare reaction generally occurs within 7 to 10 days after initiation of antiestrogen therapy and it has been shown to be predictive of response to such therapy in 80% of individuals [150–152]. Flare reaction is presumed to represent an initial agonist effect of the drug on the tumor before its antagonist effect supervenes [151].

Studies in immature female rats have shown that tamoxifen and estrogen cause similar prompt increases in FDG accumulation in an estrogen-responsive normal tissue (uterus) [153]. Presumably, both estrogen and tamoxifen initially stimulate cell proliferation and glucose metabolism and thus cause increased FDG uptake. These observations in animals suggested that augmentation of tumor FDG uptake ("metabolic flare") early during a course of tamoxifen treatment would be indicative of an agonist effect of the drug on *functional* ERs and thus predictive of a good response to therapy. To test this hypothesis, FDG-PET and FES-PET were performed in 11 patients with ER+ metastatic breast cancer before and 7 to 10 days after tamoxifen therapy. As predicted, the presence of metabolic flare, indicated by an increase in quantitative tumor FDG uptake after tamoxifen therapy over pre-therapy values, discriminated patients who subsequently responded to tamoxifen therapy from those who did not respond (see Figure 9). In addition, the pre-therapy FES uptake in the tumor and the magnitude of ER blockade by tamoxifen, as measured by a decrease in quantitative tumor FES uptake after tamoxifen therapy, were superior to *in vitro* ER and PR assays in predicting response to tamoxifen therapy [147]. These results have been confirmed in a larger series of patients with ER+ advanced breast cancer (unpublished data). This study is an example of how PET can help in managing patients with advanced breast cancer, both by identifying patients likely to benefit from hormonal therapy and by providing accurate information about the therapeutic response early after institution of such therapy.

Tumor Receptors: Summary

Clinical studies of ER imaging using FES have demonstrated PET's ability to assess ER expression in breast cancer. These studies have shown that FES-PET can identify heterogeneous expression of ER in tumors and indicate the degree of anti-estrogen blockade of the receptors. Preliminary studies have demonstrated FES-PET's potential to assess breast cancer prognosis and, combined with FDG-PET, predict tumor response to hormonal therapy. A more detailed understanding of the mechanisms important in FES uptake in breast cancer in humans, including tracer interactions with SHBG, are likely to lead to improvements in ER imaging, either through refinement of quantitative imaging approaches or the development of new ER tracers. PET imaging of PR in breast cancer and AR in prostate cancer are currently at a preclinical stage; however, ongoing testing of new radioligands and a greater understanding of factors important in steroid imaging may move these approaches into the clinical arena in the future.

Conclusions

In this review we have highlighted PET approaches to imaging cellular proliferation and hormone receptor expression. The goal is to characterize tumor biology in individual patients to guide therapy. Preliminary clinical evaluation of cellular proliferation and tumor receptor imaging methods highlight PET's ability to provide information that is not available from conventional imaging studies or from biopsy. PET tracers of cellular proliferation and tumor receptors have been designed on the basis of a large body of knowledge gained from laboratory investigations of tumor biology. This knowledge will be important in refining imaging approaches and in interpreting the results of clinical studies using these tracers.

PET imaging with FDG has improved our ability to localize cancer and therefore to direct therapy [19,20]. Promising initial results using PET to image cellular proliferation and tumor receptor expression indicate that PET's contribution to oncology does not end with FDG. In particular, PET imaging of cellular proliferation and tumor expression offers insights into the clinical biology of cancer not possible through *in vitro* analysis. Guided by ongoing research taking place at a number of centers around the world, it is likely that cellular proliferation and tumor receptor imaging will contribute to the clinical care of cancer patients, both in managing individual patients and in selecting and evaluating new agents for anti-cancer therapy.

Acknowledgements

The authors thank Kenneth Krohn, John Grierson, Timothy Tewson, and Janet Eary for helpful comments.

References

[1] Tannock IF, and Hill RP (1992). *The Basic Science of Oncology*, McGraw-Hill, New York.
[2] Sledge GJ, and McGuire W (1983). Steroid hormone receptors in human breast cancer. *Adv Cancer Res* **38**, 61–75.
[3] McGuire W, and Horwitz K (1975). Predicting response to endocrine therapy in human breast cancer: a hypothesis. *Science* **189**, 726–727.
[4] Muss H, Thor A, Berry D, *et al.* (1994). C-erbB-2 expression and response to adjuvant therapy in women with node-positive early breast cancer. *N Engl J Med* **330**, 1260–1266.
[5] Vollenweider-Zerargui L, Barrelet L, Wong Y, Lemarchand-Beraud T, and Gomez F (1986). The predictive value of estrogen and

progesterone receptors' concentrations on the clinical behavior of breast cancer in women: clinical correlation on 547 patients. *Cancer* **57**, 1170–1180.

[6] Livingston R, and Ellis G (1995). Breast cancer: dose response and intensity. *Cancer Chemother* **10**, 17–26.

[7] Hoehn J, Plotka E, and Dickson K (1979). Comparison of estrogen receptor levels in primary and regional metastatic carcinoma of the breast. *Ann Surg* **190**, 69–71.

[8] Holdaway I, and Bowditch J (1983). Variation in receptor status between primary and metastatic breast cancer. *Cancer* **52**, 479–485.

[9] Kamby C, Rasmussen BB, and Kristensen B (1989). Oestrogen receptor status of primary breast carcinomas and their metastases. Relation to pattern of spread and survival after recurrence. *Br J Cancer* **60**, 252–257.

[10] Husband JE (1996). Monitoring tumor response. *Eur Radiol* **6**, 775–785.

[11] Radford JA, Cowan RA, Flanagan M, *et al.* (1989). The significance of residual mediastinal abnormality on the chest radiograph following treatment for Hodgkin's disease. *J Clin Oncol* **6**, 940–946.

[12] Feldman LD, Hortobagyi GN, Buzdar AU, Ames FC, and Blumenschein GR (1986). Pathological assessment of response to induction chemotherapy in breast cancer. *Cancer Res* **46**, 2578–2581.

[13] Livingston RB, and Hart JS (1977). The clinical applications of cell kinetics in cancer therapy. *Annu Rev Toxicol* **17**, 529–543.

[14] Chang J, Powles T, Allred D, *et al.* (1999). Biologic markers as predictors of clinical outcome from systemic therapy for primary operable breast cancer. *J Clin Oncol* **17**, 3058–3063.

[15] Katzenellenbogen JA, Coleman RE, Hawkins RA, *et al.* (1995). Tumor receptor imaging: proceedings of the National Cancer Institute workshop, review of current work, and prospective for further investigations. *Clin Cancer Res* **1**, 921–932.

[16] Strauss L, and Conti P (1991). The application of PET in clinical oncology. *J Nucl Med* **32**, 623–647.

[17] Jones T (1996). The role of positron emission tomography within the spectrum of medical imaging. *Eur J Nucl Med* **23**, 207–211.

[18] Shields AF, Graham MM, and Spence AM (1995). The role of PET imaging in clinical oncology. In *Nuclear Medicine Annual 1995*. LM Freeman (Ed). Raven Press, New York. pp. 129–168.

[19] Rigo P, Paulus P, Kaschten BJ, *et al.* (1996). Oncological applications of positron emission tomography with fluoro-D-glucose. *Eur J Nucl Med* **23**, 1641–1674.

[20] Eary J (1999). Nuclear medicine in oncology diagnosis. *Lancet* **354**, 853–857.

[21] Reivich M, Alavi A, Wolf A, *et al.* (1985). Glucose metabolic rate kinetic model parameter determination in humans: the lumped constant and rate constants for fluoro-D-glucose and [^{11}C]deoxyglucose. *J Cereb Blood Flow Metab* **5**, 179–192.

[22] Sokoloff L, Reivich M, Kennedy C, *et al.* (1977). The [^{14}C]deoxyglucose method for the measurement of local cerebral glucose utilization: theory, procedure, and normal values in the conscious and anesthetized albino rat. *J Neurochem* **28**, 897–916.

[23] Smith TA (1998). FDG uptake, tumor characteristics and response to therapy: a review. *Nucl Med Commun* **19**, 97–105.

[24] Strauss L (1996). Fluorine-18 deoxyglucose and false-positive results:a major problem in the diagnostics of oncological patients. *Eur Journal Nucl Med* **23**, 1409–1415.

[25] Strauss LG (1997). Positron emission tomography: a current role for diagnosis and therapy monitoring in oncology. *Oncologist* **2**, 381–388.

[26] Shields AF, Ho PT, and Grierson JR (1999). The role of imaging in the development of oncologic agents. *J Clin Pharmacol* **39**, Suppl, 40S–44S.

[27] Price P, and Jones T (1995). Can positron emission tomography (PET) be used to detect subclinical response to cancer therapy? The EC PET oncology concerted action and the EORC PET study group. *Eur J Cancer* **31**, 1924–1927.

[28] Huovinen R, Leskinen-Kallo S, Nagren K, *et al.* (1993). Carbon-11-methionine and PET in evaluation of treatment response of breast cancer. *Br J Cancer* **67**, 787–791.

[29] Kole A, Pruim J, Nieweg O, *et al.* (1997). PET with L-[1-carbon-11]-tyrosine to visualize tumors and measure protein synthesis rates. *J Nucl Med* **38**, 191–195.

[30] Hara T, Kosaka N, Shinoura N, and Kondo T (1997). PET imaging of brain tumor with [methyl–^{11}C]choline. *J Nucl Med* **38**, 842–847.

[31] Rasey JS, Koh W, Grierson JR, Grunbaum Z, and Krohn KA (1989). Radiolabeled fluoromisonidazole as an imaging agent for tumor hypoxia. *Int J Radiat Oncol Biol Phys* **17**, 985–992.

[32] Andrich MP, and Neumann R (1994). The role of positron emission tomography imaging in early assessment of the antitumor impact on biologics and cytotoxics. *Curr Opin Oncol* **6**, 627–632.

[33] Price P, Harte R, Wells P, *et al.* (1997). The potential of tracer kinetic studies in drug development programs: a new investigational area for cancer research. *Drug Inf J* **31**, 1045–1049.

[34] Tannock IF (1992). Cell proliferation. In *The Basic Science of Oncology*. IF Tannock, and RP Hill (Eds). McGraw-Hill, New York. pp. 154–177.

[35] Cleaver JE (1967). Thymidine metabolism and cell kinetics. *Front Biol* **6**, 43–100.

[36] Wohlhueter RM, Marz R, and Plagemann PG (1979). Thymidine transport in cultured mammalian cells. Kinetic analysis, temperature dependence and specificity of the transport system. *Biochim Biophys Acta* **553**, 262–283.

[37] Livingston RB, Ambus U, George SL, Freireich EJ, and Hart JS (1974). *In vitro* determination of thymidine-[H-3] labeling index in human solid tumors. *Cancer Res* **34**, 1376–1380.

[38] Christman D, Crawford EJ, Friedkin M, and Wolf AP (1972). Detection of DNA synthesis in intact organisms with positron-emitting methyl-[C-11]-thymidine. *Proc Natl Acad Sci U S A* **69**, 988–992.

[39] Sundoro-Wu BM, Schmall B, Conti PS, *et al.* (1984). Selective alkylation of pyrimidyl-dianions: synthesis and purification of ^{11}C labeled thymidine for tumor visualization using Positron Emission Tomography. *Int J Appl Radiat Isot* **35**, 705–708.

[40] Vander Borght T, Labar D, Pauwels S, and Lambotte L (1991). Production of [2-^{11}C]thymidine for quantification of cellular proliferation with PET. *Appl Radiat Isot* **42**, 103–104.

[41] Link JM, Grierson J, and Krohn K (1995). Alternatives in the synthesis of 2-[C-11]-thymidine. *J Labelled Compd Radiopharm* **37**, 610–612.

[42] Conti PS, Hilton J, Wong DF, *et al.* (1994). High performance liquid chromatography of carbon-11 labeled thymidine and its mjor carabolites for clinical PET studies. *Nucl Med Biol* **21**, 1045–1051.

[43] Goethals P, Eijkeren Mv, Lodewyck W, and Dams R (1995). Measurement of [methyl-carbon-11]thymidine and its metabolites in head and neck tumors. *J Nucl Med* **36**, 880–882.

[44] Goethals P, Lameire N, van Eijkeren M, *et al.* (1996). [Methyl-carbon-11]thymidine for *in vivo* measurement of cell proliferation. *J Nucl Med* **37**, 1048–1052.

[45] Shields AF, Mankoff DA, Graham MM, *et al.* (1996). Analysis of 2-[C-11]-thymidine blood metabolites in PET imaging. *J Nucl Med* **37**, 290–296.

[46] Shields AF, Graham MM, Kozawa SM, *et al.* (1992). Contribution of labeled carbon dioxide to PET imaging of carbon-11-labeled compounds. *J Nucl Med* **33**, 581–584.

[47] Siesjo BK, and Thompson WOB (1965). The uptake of inspired [C-14]-CO_2 into the acid-labile, the acid-soluble, the lipid, the protein and the nucleic acid fractions of rat brain tissue. *Acta Physiol Scand* **64**, 182–192.

[48] Lockwood AH, and Finn RD (1982). [C-11]-carbon dioxide fixation and equilibration in rat brain: effects on acid–base measurements. *Neurology* **32**, 451–454.

[49] Shields AF, Lim K, Grierson J, Link J, and Krohn KA (1990). Utilization of labeled thymidine in DNA synthesis: studies for PET. *J Nucl Med* **31**, 337–342.

[50] Mankoff DA, Shields AF, Graham MM, *et al.* (1998). Kinetic analysis of 2-[carbon-11]thymidine PET imaging studies: compartmental model and mathematical analysis. *J Nucl Med* **39**, 1043–1055.

[51] Guenther I, Wyer L, Knust EJ, *et al.* (1998). Radiosynthesis and quality assurance of 5-[^{124}I]-iodo-2′-deoxyuridine for functional PET imaging of cell proliferation. *Nucl Med Biol* **25**, 359–365.

[52] Bergstrom M, Lu L, Fasth KJ, *et al.* (1998). *In vitro* and animal validation of bromine-76-bromodeoxyuridine as a proliferation marker. *J Nucl Med* **39**, 1273–1279.

[53] Tjuvajev J, Muraki A, Ginos J, *et al.* (1993). Iododeoxyuridine uptake and retention as a measure of tumor growth. *J Nucl Med* **34**, 1152–1162.

[54] Tjuvajev JG, Macapinlac HA, Daghighian F, *et al.* (1994). Imaging of brain tumor proliferative activity with iodine-131-iododeoxyuridine. *J Nucl Med* **35**, 1407–1417.

[55] Kassis AI, Adelstein SJ, and Mariani G (1996). Radiolabeled nucleoside analogs in cancer diagnosis therapy. *Q J Nucl Med* **40**, 301–319.

[56] Abe Y, Fukuda H, Ishiwata K, *et al.* (1983). Studies on ^{18}F-labeled pyrimidines. Tumor uptakes of ^{18}F-5-fluorouracil, ^{18}F-5-fluorour-

idine, and ^{18}F-5-fluoro-2′-deoxyuridine in animals. *Eur J Nucl Med* **8**, 258–261.

[57] Fowler JS, Finn RD, Lambrecht RM, and Wolf AP (1973). The synthesis of ^{18}F-5-fluorouracil. VII. *J Nucl Med* **14**, 63–64.

[58] Crawford EJ, Friedkin M, Wolf AP, *et al.* (1982). ^{18}F-5-fluorouridine, a new probe for measuring the proliferation of tissue *in vivo*. *Adv Enzyme Regul* **20**, 3–22.

[59] Washtien WL, and Santi DV (1979). Assay of intracellular free and macromolecular-bound metabolites of 5-fluorodeoxyuridine and 5-fluorouracil. *Cancer Res* **39**, 3397–3404.

[60] Grierson JR, Shields AF, Zheng M, Kozawa SM, and Courter JH (1995). Radiosynthesis of labeled β-pseudothymidine ([C-11]- and [H-3]-*methyl*) and its biodistribution and metabolism in normal and tumored mice. *Nuclear Med Biol* **22**, 671–678.

[61] Shields AF, Grierson JR, Kozawa SM, and Zheng M (1996). Development of labeled thymidine analogs for imaging tumor proliferation. *Nucl Med Biol* **23**, 17–22.

[62] Phillips FS, Feinberg A, Chou T-C, *et al.* (1983). Distribution, metabolism, and excretion of 1-(2-fluoro-2-deoxy-β-D-arabinofuranosyl)thymine and 1-(2-fluoro-2-deoxy-β-D-arabinofuranosyl)-5-idocytosine. *Cancer Res* **43**, 3619–3627.

[63] Conti PS, Allauddin MM, Fissekis JR, Schmall B, and Watnabe KA (1995). Synthesis of 2′-fluoro-5-methyl-1-beta-D-arabinofuranosyluracil ([^{11}C]-FMAU): a potential nucleoside analog for *in vivo* study of cellular proliferation with PET. *Nucl Med Biol* **22**, 783–789.

[64] Conti P, Alauddin MM, Fissekis JD, and Wanatabe KA (1999). Synthesis of [F-18]-2-fluoro-5-methyl-1-β-D-arabinofuranosyluracil ([F-18]FMAU) (abstract). *J Nucl Med* **40**, 83P.

[65] Flexner C, van der Horst C, Jacobson MA, *et al.* (1994). Relationship between plasma concentrations of 3′-deoxy-3′-fluorothymidine (alovudine) and antiretroviral activity in two concentration-controlled trials. *J Infect Dis* **170**, 1394–1403.

[66] Munch-Petersen B, Cloos L, Tyrsted G, and Eriksson S (1991). Diverging substrate specificity of pure human thymidine kinases 1 and 2 against antiviral dideoxynucleosides. *J Biol Chem* **266**, 9032–9038.

[67] Shields AF, Grierson JR, Dohmen BM, *et al.* (1998). Imaging proliferation *in vivo* with [F-18]FLT and positron emission tomography. *Nat Med* **4**, 1334–1336.

[68] Larson SM, Weiden PL, Grunbaum Z, *et al.* (1981). Positron imaging feasibility studies I: characteristics of [H-3]-thymidine uptake in rodent and canine neoplasms: concise communication. *J Nucl Med* **22**, 869–874.

[69] Shields AF, Larson SM, Grunbaum Z, and Graham MM (1984). Short-term uptake in normal and neoplastic tissues: studies for PET. *J Nucl Med* **25**, 759–764.

[70] Schmall B, Conti P, Schaeffer D, and Kleinert E (1992). Tumor and organ biochemical profiles *in vivo* following uptake of a combination of radiolabeled substrates: a potential application for PET. *Am J Physiol Imaging* **7**, 2–11.

[71] Tew KD, and Taylor DM (1978). The relationship of thymidine metabolism to the use of fractional incorporation as a measure of DNA synthesis in tissue proliferation. *Eur J Cancer* **14**, 153–168.

[72] Higashi K, Clavo AC, and Wahl RL (1993). *In vitro* assessment of 2-fluoro-2-deoxy-D-glucose, L-methionine and thymidine as agents to monitor the early response of a human adenocarcinoma cell line to radiotherapy. *J Nucl Med* **34**, 773–779.

[73] Kubota K, Ishitawa K, Kubota R, *et al.* (1991). Tracer feasability for monitoring tumor radiotherapy: a quadruple tracer study with fluoro-D-glucose or fluorine-18-fluorodeoxyuridine, L-[methyl-^{14}C]methionine, [6-^{3}H]thymidine, and gallium-67. *J Nucl Med* **32**, 2118–2123.

[74] Kuebbing D, and Werner R (1975). A model for compartmentation of *de novo* and salvage thymidine nucleotide pools in mammalian cells. *Proc Natl Acad Sci U S A* **72**, 3333–3336.

[75] Shields AF, Coonrod DV, Quackenbush RC, and Crowley JJ (1987). Cellular sources of thymidine nucleotides: studies for PET. *J Nucl Med* **28**, 1435–1440.

[76] Martiat P, Ferrant A, Lambar D, *et al.* (1988). *In vivo* measurement of carbon-11 thymidine uptake in non-Hodgkin's lymphoma using positron emission tomography. *J Nucl Med* **29**, 1633–1637.

[77] van Eijkeren M, Schryver AD, Goethals P, *et al.* (1992). Measurement of short-term ^{11}C-thymidine activity in human head and neck tumors using positron emission tomography (PET). *Oncol* **31**, 539–543.

[78] Mankoff DA, Shields AF, Link JM, *et al.* (1999). Kinetic analysis of 2-[C-11]thymidine PET imaging studies: validation studies. *J Nucl Med* **40**, 614–624.

[79] Patlak C, Dhawan V, Takikawa S, *et al.* (1993). Estimation of striatal uptake rate constant of FDOPA using PET: methodologic issues. In *Quantification of Brain Function. Tracer Kinetics and Image Analysis in Brain PET*. K Uemera, *et al.* (Eds). Elsevier Science Publishers, Amsterdam, Netherlands.

[80] Mankoff DA, Shields AF, Graham MM, Link JM, and Krohn KA (1996). A graphical analysis method to estimate blood–tissue transfer constants for systems with labeled metabolites. *J Nucl Med* 37.

[81] Cunningham V, Ashburner J, Byrne H, and Jones T (1993). Use of spectral analysis to obtain images from dynamic PET studies. In *Quantification of Brain Function: Tracer Kinetics and Image Analysis in PET*. Uemera K, *et al.* (Eds). Elsevier, Amsterdam. pp. 101–108.

[82] Young H, Brock C, Wells P, and Price P (1999). Monitoring response to treatment in the development of anti-cancer drugs using positron emission tomography (PET). *Drug Inf J* **33**, 237–244.

[83] Cunningham V, and Jones T (1993). Spectral analysis of dynamic PET studies. *J Cereb Blood Flow Metab* **13**, 15–23.

[84] O'Sullivan F (1993). Imaging radiotracer model parameters in PET: a mixture analysis approach. *IEEE Trans Med Imag* **12**, 399–412.

[85] Eary JF, Mankoff DA, Spence AM, *et al.* (1999). 2-[C-11]-thymidine imaging of malignant brain tumors. *Cancer Res* **59**, 615–621.

[86] Cornford EM, and Oldendorf WH (1975). Independent blood–brain barrier transport systems for nucleic acid precursors. *Biochim et Biophys Acta* **394**, 211–219.

[87] Kriss JP, Maruyama Y, Tung LA, Bond SB, and Revesz L (1963). The fate of 5-bromodeoxycytodine and 5-iododeoxyruridine in man. *Cancer Res* **23**, 260–273.

[88] Philip PA, Bagshawe KD, Searle F, *et al.* (1991). *In vivo* uptake of ^{131}I-5-iodo-2-deoxyuridine by malignant tumours in man. *Br J Cancer* **63**, 134–135.

[89] van Eijkeren ME, Thierens H, Seuntjens J, *et al.* (1996). Kinetics of [methyl-^{11}C]thymidine in patients with squamous cell carcinoma of the head and neck. *Acta Oncol* **35**, 737–741.

[90] De Reuck J, Santens P, Goethals P, *et al.* (1999). [Methyl-^{11}C]thymidine positron emission tomography in tumoral and non-tumoral cerebral lesions. *Acta Neurol Belg* **99**, 118–125.

[91] Shields AF, Mankoff DA, Link JM, *et al.* (1998). Carbon-11-thymidine and FDG to measure therapy response. *J Nucl Med* **39**, 1757–1762.

[92] Vander Borght T, Pauwels S, Lambotte L, *et al.* (1994). Brain tumor imaging with PET and 2-[carbon-11]thymidine. *J Nucl Med* **35**, 974–982.

[93] Santen RJ, Manni A, Harvey H, and Redmond C (1990). Endocrine treatment of breast cancer in women. *Endocr Rev* **11**, 221–265.

[94] Blankenstein MA B-dVJ, van Aubel OG, van Steenbrugge GJ (1988). Hormone receptors in human prostate cancer. *Scan J Urol Nephrol* **107**, 39–45.

[95] Brennan M, Donegan W, and Appleby D (1979). The variability of estrogen receptors in metastatic breast cancer. *Am J Surg* **137**, 260–262.

[96] McCarty KS, Miller LS, Cox EB, Konrath J, and McCarty KS (1985). Estrogen receptor analyses. Correlation of biochemical and immunohistochemical methods using monoclonal antireceptor antibodies. *Arch Pathol Lab Med* **109**, 716–721.

[97] Hull D, Clark G, Osborne C, *et al.* (1983). Multiple estrogen receptor assays in human breast cancer. *Cancer Res* **43**, 413–416.

[98] Barrack ER, and Tindall DJ (1987). A critical evaluation of the use of androgen receptor assays to predict the androgen responsiveness of prostatic cancer. In *Current Concepts and Approaches to the Study of Prostatic Cancer*. D Coffey (Ed). Alan R. Liss, New York. pp. 155–187.

[99] Ekman P, Dahlberg E, Gustafsson J, *et al.* (1980). Present and future clinical value of steroid receptor assays in human prostatic carcinoma. In *Hormones and Cancer*. S Lacobelli (Ed). Raven Press, New York, NY. pp. 361–370.

[100] Katzenellenbogen J (1981). The development of gamma-emitting hormone analogs as imaging agents for receptor-positive tumors. In *The Prostatic Cell: Structure and Function Part B*. G Murphy, and A Sandberg (Eds). Alan R. Liss, New York. pp. 313–327.

[101] Sadi M, and Barrack E (1993). Image analysis of androgen receptor immunostaining in metastatic prostate cancer: heterogeneity as a predictor of response to hormonal therapy. *Cancer* **71**, 2574–2580.

[102] Smith DC (1999). Chemotherapy for hormone refractory prostate cancer. *Urol Clin North Am* **26**, 323–331.

[103] Isaacs JT (1999). The biology of hormone refractory prostate cancer. How does it develop? *Urol Clin North Am* **26**, 323–331.

[104] Katzenellenbogen JA, Welch MJ, and Dehdashti F (1997). The development of estrogen and progestin radiopharmaceuticals for imaging breast cancer. *Anticancer Res* **17**, 1573–1576.

[105] Katzenellenbogen J (1992). The pharmacology of steroid radiopharmaceuticals: specific and non-specific binding and uptake selectivity. In *Radiopharmaceuticals: Chemistry and Pharmacology.* A Nunn (Ed). Marcel Dekker, New York. pp. 297–331.

[106] VanBrocklin HF, Pomper MG, Carlson KE, Welch MJ, and Katzenellenbogen JA (1992). Preparation and evaluation of 17-ethynyl-substituted 16-α-[^{18}F]fluoroestradiols: selective receptor-based PET imaging agents. *Int J Rad Appl Instrum Part B* **19**, 363–374.

[107] VanBrocklin HF, Rocque PA, Lee HV, *et al.* (1993). 16β-[^{18}F]fluoromoxestrol: a potent, metabolically stable positron emission tomography imaging agent for estrogen receptor positive human breast tumors. *Life Sci* **53**, 811–819.

[108] Katzenellenbogen J, Heiman D, Senderoff S, *et al.* (1982). Estrogen receptor-based agents for imaging breast tumors: binding selectivity as a basis for design and optimization. In *Applications of Nuclear and Radiochemistry.* N Morcos, and R Lambrecht (Eds). Pergamon Press, New York. pp. 311–323.

[109] Buckman B, Bonasera T, Kirschbaum K, Welch M, and Katzenellenbogen J (1995). Fluorine-18-labeled progestin 16α, 17α-dioxolanes: development of high-affinity ligands for the progesterone receptor with high *in vivo* target site selectivity. *J Med Chem* **38**, 328–337.

[110] Kilbourn M, and Zalutsky M (1985). Research and clinical potential of receptor based radiopharmaceuticals. *J Nucl Med* **26**, 655–662.

[111] Brandes S, and Katzenellenbogen J (1988). Fundamental considerations in the design of fluorine-18 labeled progestins and androgens as imaging agents for receptor-positive tumors of the breast and prostate. *Radiat Appl Instrum* **15**, 53–67.

[112] Hammond G (1993). Steroid hormone action. In *Extracellular Steroid-Binding Proteins.* M Parker (Ed). Oxford University Press, New York. pp. 210.

[113] Tait J, and Tait S (1991). The effect of plasma protein binding on the metabolism of steroid hormones. *J Endocrinol* **131**, 339–357.

[114] Petra P (1991). The plasma sex steroid binding protein (SBP or SBHG). A critical review of recent developments on the structure, molecular biology and function. *J Steroid Biochem Mol Biol* **40**, 735–753.

[115] Hyrb D, Khan M, Romas N, and Rosner W (1990). The control of the interaction of sex hormone-binding globulin with its receptor by steroid hormones. *J Biol Chem* **265**, 948–954.

[116] Hobbs C, Jones R, and Plymate S (1992). The effects of sex hormone-binding globulin (SHBG) on testosterone transport into the cerebrospinal fluid. *J Steroid Biochem Mol Biol* **42**, 629–635.

[117] Eckelman W (1992). The development of single-photon emitting receptor-binding radiotracers. In *Radiopharmaceuticals: Chemistry and Pharmacology.* A Nunn (Ed). Marcel Dekker, New York. pp. 167–219.

[118] Cummins C (1993). Radiolabeled steroidal estrogen in cancer research. *Steroids* **58**, 245–259.

[119] Katzenellenbogen J, Hsiung H, Carlson K, *et al.* (1975). Iodohexestrols II. Characterization of the binding and estrogenic activity of iodinated hexestrol derivatives *in vitro* and *in vivo*. *Biochemistry* **14**, 1742–1750.

[120] McElvany KD, Katzenellenbogen JA, Shafer KE, *et al.* (1982). 16α-[^{77}Br]bromoestradiol: dosimetry and preliminary clinical studies. *J Nucl Med* **23**, 425–430.

[121] Landvatter S, Kiesewetter D, Kilbourn M, Katzenellenbogen J, and Welch M (1983). (2*R**, 3*S**)-1-[^{18}F]fluoro-2,3-bis(4-hydroxyphenyl)pentane ([^{18}F]fluorononorhexestrol): a positron-emitting estrogen that shows highly selective, receptor-mediated uptake by target tissues *in vivo*. *Life Sci* **33**, 1933–1938.

[122] Kiesewetter DO, Kilbourn MR, Landvatter SW, *et al.* (1984). Preparation of four fluorine-18-labeled estrogens and their selective uptakes in target tissue of immature rats. *J Nucl Med* **25**, 1212–1221.

[123] Kieswetter D, Katzenellenbogen J, Kilbourn M, and Welch M (1984). Synthesis of 16-fluoroestrogens by unusually facile fluoride ion displacement reactions: prospects for the preparation of fluorine-18 labeled estrogens. *J Org Chem* **49**, 4900–4905.

[124] Brodack J, Kilbourn M, and Welch M (1986). Application of robotics to radiopharmaceutical preparation: controlled synthesis of fluorine-18 16α-fluoroestradiol-17β. *J Nucl Med* **27**, 714–721.

[125] Tewson TJ (1995). The routine synthesis of fluorine-18 16α-fluoroestradiol: the use of 3-methoxymethyl-epiestriol-16β,17β-cyclic sulfate as the starting substrate. *J Labelled Compd Radiopharm* **37**, 589–591.

[126] Romer J, Fuchtner J, Steinback J, Johansnsen B, and Forschungzentrum R (1999). Automated Production of 16α-[^{18}F]Fluoroesrtradiol for breast cancer imaging. *Nucl Med Biol* **26**, 473–479.

[127] Jonson SD, and Welch MJ (1998). PET imaging of breast cancer with fluorine-18 radiolabeled estrogens and progestins. *Q J Nucl Med* **42**, 8–17.

[128] Jonson SD, Bonasera TA, Dehdashti F, *et al.* (1999). Comparative breast tumor imaging and comparative *in vitro* metabolism of 16α-[^{18}F]fluoroestradiol-17β and 16β-[^{18}F]fluoromoxestrol in isolated hepatocytes. *Nucl Med Biol* **26**, 123–130.

[129] Yang D, Kuang LR, Cherif A, *et al.* (1993). Synthesis of [^{18}F]fluoroalanine and [^{18}F]flourotamoxifen for imaging breast tumors. *J Drug Target* **1**, 259–267.

[130] Yang DJ, Li C, Kuang LR, *et al.* (1994). Imaging, biodistribution and therapy potential of halogenated tamoxifen analogues. *Life Sci* **55**, 53–67.

[131] Pomper MG, Katzenellenbogen JA, Welch MJ, Brodack JW, and Mathias CJ (1988). 21-[^{18}F]fluoro-16 α-ethyl-19-norprogesterone: syntheses and target tissue selective uptake of a progestin receptor for positron emission tomography. *J Med Chem* **31**, 1360–1363.

[132] Pomper M, Pinney K, Carlson K, and *et al.* (1990). Target tissue uptake selectivity of three fluorine-substituted progestins: potential imaging agents for receptor-positive breast tumors. *Nucl Med Biol* **17**, 309–319.

[133] Verhagen A, Elsinga PH, Groot TJd, *et al.* (1991). A fluorine-18 labeled progestin as an imaging agent for progestin receptor positive tumors with positron emission tomography. *Cancer Res* **51**, 1930–1933.

[134] Kontula K, Jänne O, Vihko R, *et al.* (1975). Progesterone-binding proteins: *in vitro* binding and biological activity of different steroidal ligands. *Acta Endocrinol* **78**, 574–592.

[135] Verhagen A, Studeny M, Luurtsema G, *et al.* (1994). Metabolism of a [^{18}F]fluorine labeled progestin (21-[^{18}F]fluoro-16 alpha-ethyl-19-norprogesterone) in humans: a clue for future investigations. *Nucl Med Biol* **21**, 941–952.

[136] Dehdashti F, McGuire AH, Brocklin HFV, *et al.* (1991). Assessment of 21-[^{18}F]fluoro-16 alpha-ethyl-19-nonprogesterone as a positron-emitting radiopharmaceutical for the detection of progestin receptors in human breast carcinomas. *J Nucl Med* **32**, 1532–1537.

[137] Liu A, Dence C, Welch M, and Katzenellenbogen J (1992). Fluorine-18-labeled androgens: radiochemical synthesis and tissue distribution studies on six fluorine-substituted androgens, potential imaging agents for prostatic cancer. *J Nucl Med* **33**, 724–734.

[138] Bonasera T, O'Neil J, Xu M, *et al.* (1996). Preclinical evaluation of fluorine-18-labeled androgen receptor ligands in baboons. *J Nucl Med* **37**, 1009–1015.

[139] Mathias CJ, Welch MJ, Katzenellenbogen JA, *et al.* (1987). Characterization of the uptake of 16 alpha-([^{18}F]fluoro)-17 beta-estradiol in DMBA-induced mammary tumors. *Int J Radiat Appl Instrum* **14**, 15–25.

[140] Mintun MA, Welch MJ, Siegel BA, *et al.* (1988). Breast cancer: PET imaging of estrogen receptors. *Radiology* **169**, 45–48.

[141] Katzenellenbogen JA, Mathias CJ, Vanbrocklin HF, Brodack JW, and Welch MJ (1993). Titration of the *in vivo* uptake of 16alpha-[F-18]fluoroestradiol by target tissues in the rat: competition by tamoxifen, and implications for quantitating estrogen receptors *in vivo* and the use of animal models in receptor-binding radiopharmaceutical development. *Nucl Med Biol* **20**, 735–745.

[142] Mankoff DA, Tewson TJ, and Eary JF (1997). Analysis of blood clearance and labeled metabolites for the estrogen receptor tracer [^{18}F]-16 alpha-fluoroestradiol (FES). *Nucl Med Biol* **24**, 341–348.

[143] Moresco RM, Scheithauer BW, Lulcignani G, *et al.* (1997). Oestrogen receptors in meningiomas: a correlative pet and immunohistochemical study. *Nucl Med Commun* **18**, 606–615.

[144] Tewson T, Mankoff D, Peterson L, Woo I, and Petra P (1999). The interactions of 16α-[F-18]-fluoroestradiol (FES) with sex steroid binding protein (SBP). *Nucl Med Biol* in press.

[145] Reventos J, Sullivan P, Joseph D, and Gordon J (1993). Tissue-specific expression of the rat androgen-binding protein/sex hormone-binding globulin gene in transgenic mice. *Mol Cell Endocrinol* **96**, 69–73.

[146] Dehdashti F, Mortimer JE, Siegel BA, *et al.* (1995). Positron tomographic assessment of estrogen receptors in breast cancer: a comparison with FDG-PET and *in vitro* receptor assays. *J Nucl Med* **36**, 1766–1774.

[147] Dehdashti F, Flanagan FL, Mortimer JE, *et al.* (1999). Positron emission tomographic assessment of "metabolic flare" to predict response of metabolic breast cancer to antiestrogen therapy. *Eur J Nucl Med* **26**, 51–56.

[148] McGuire AH, Dehdashti F, Siegel BA, *et al.* (1991). Positron tomographic assessment of 16 alpha-[^{18}F] fluoro-17 beta-estradiol uptake in the metastatic breast carcinoma. *J Nucl Med* **32**, 1526–1531.

[149] Mortimer JE, Dehdashti F, Siegel BA, *et al.* (1996). Positron emission tomography with 2-[^{18}F]fluoro-2-deoxy-D-glucose and 16alpha-[^{18}F]fluoro-17beta-estradiol in breast cancer: correlation with estrogen receptor status and response to systemic therapy. *Clin Cancer Res* **2**, 933–939.

[150] Plotkin D, Lechner JJ, Jung WE, and *et al.* (1978). Tamoxifen flare in advanced breast cancer. *JAMA* **240**, 2644–2646.

[151] Legha S (1988). Tamoxifen in the treatment of breast cancer. *Ann Intern Med* **109**, 219–228.

[152] Vogel CL, Schoenfelder J, Shemano I, and *et al.* (1995). Worsening bone scan in the evaluation of antitumor response during hormonal therapy of breast cancer. *J Clin Oncol* **13**, 1123–1128.

[153] Welch M, Bonasera T, Sherman E, and *et al.* (1995). fluoro-D-glucose (FDG) and 16α[F-18]fluoroestradiol-17β (FES) uptake in estrogen-receptor (ER)-rich tissues following tamoxifen treatment: a preclinical study (abstract). *J Nucl Med* **36**, 39P.